

Measurement of Nitrogen II and Carbon II Resonance Multiplet Line Shapes From a Plasma

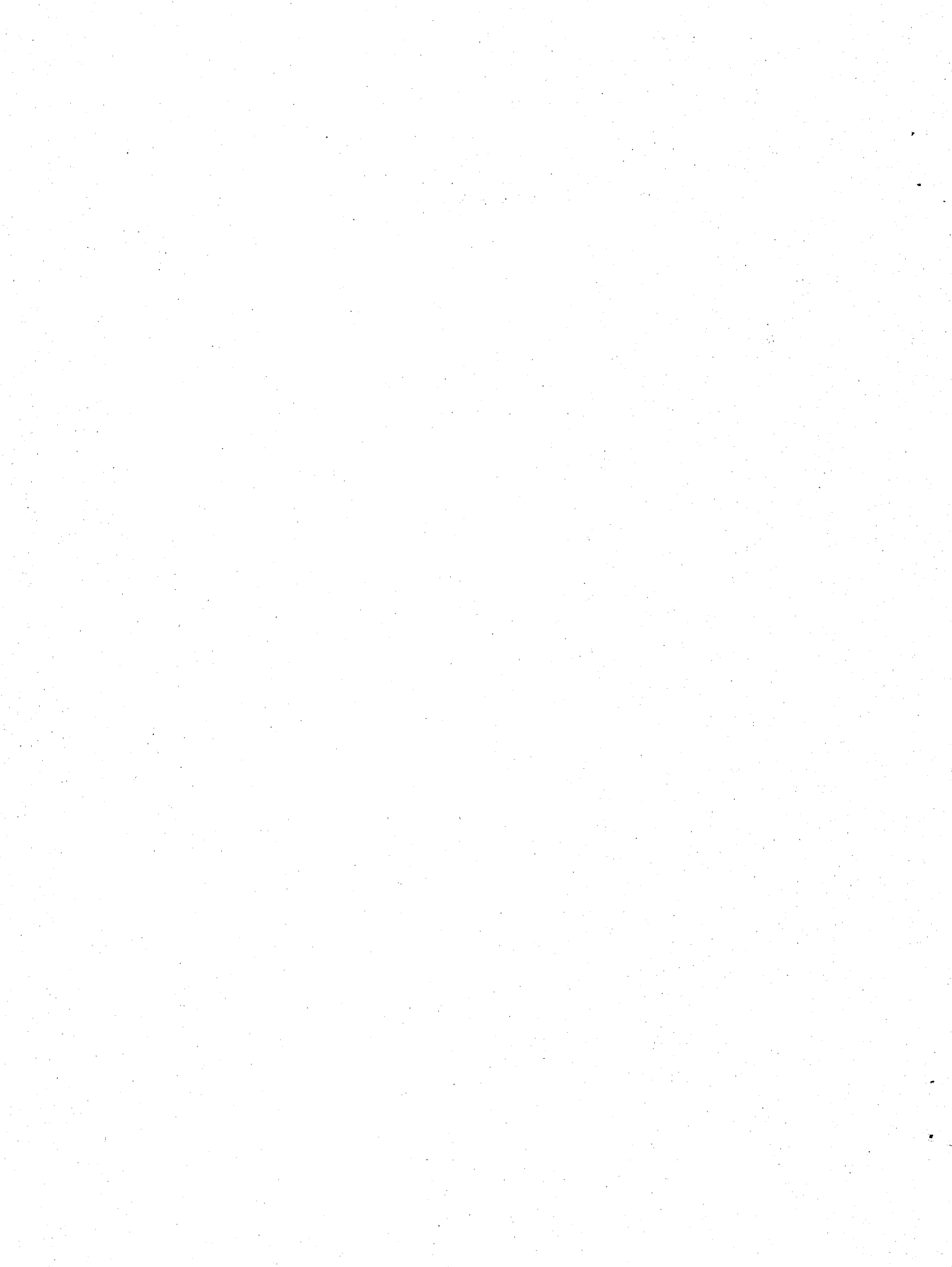
JOHN D. E. FORTNA

*High Temperature Physics Branch
Plasma Physics Division*

December 31, 1969



NAVAL RESEARCH LABORATORY
Washington, D.C.



ABSTRACT

The spectral line shapes of the Nitrogen II and Carbon II resonance multiplets, which occur in the vacuum ultraviolet region of the spectrum, have been measured. The Stark widths were deduced from the optically thin Lorentz wings. The source of radiation was a hot plasma produced by reflecting the shock wave generated by an electromagnetic T-type shock tube operating at a moderate pressure of helium gas to which the test elements (and hydrogen) were added. The electron temperature was determined from the ratio of the total intensities of the He I 4713 Å and the H β 4861 Å lines. The electron density was obtained from the halfwidth of the He I 3889 Å line. Measurement of the electron temperature and density of the test plasma was such as to provide a critical test of a recent semiempirical theory of Stark broadening of isolated ion lines under conditions in which the broadening electron collisions are predominantly elastic and without classical analogue. Agreement with the theory was found to within the expected precision of the theory.

PROBLEM STATUS

This is a final report on one phase of a continuing study of line broadening and radiative transfer in plasmas.

AUTHORIZATION

NRL Problem H02-24
Project RR-002-09-41-5054

Manuscript submitted June 20, 1969.

ACKNOWLEDGMENTS

I gratefully acknowledge the guidance of Prof. H. R. Griem who suggested the topic for this report, and the support of the Naval Research Laboratory which provided the facilities for this research. The encouragement of Dr. A. C. Kolb and the valuable consultations with Dr. R. C. Elton are deeply appreciated.

I wish to thank Dr. J. R. Greig for his helpful suggestions and for providing me with the temperature computations. I am also grateful to Dr. Roger Bengtson for providing me with the Rankine-Hugoniot calculations.

The fine craftsmanship of Mr. Leonard Melhart in the design of the shock tube T-section and of Mr. Harry Hoyle of the NRL Sheet Metal Shop in the construction of the gas mixing system is reflected in the trouble free performance of these components over thousands of firings. The technical assistance unstintingly supplied by Mr. Morton Fink in the face of more pressing responsibilities is gratefully recalled.

The able assistance of Messrs. Edward Laikin, Stuart Hauver, Kent Gerber, Earl Warden and Louis Verna during the long and late data runs is greatly appreciated, and especially valuable were the many computations of

TABLE OF CONTENTS

Chapter	Page
I. INTRODUCTION	1
A. Preliminary Discussion.	1
B. Survey of Recent Theory and Experiments	4
C. The Semiempirical Approximation	9
D. Purpose of the Experiment.	14
E. Validity of the Approximations	15
II. DIAGNOSTIC THEORY	19
A. Spectroscopic Theory	19
B. LTE and Rankine-Hugoniot Comparison	24
III. APPARATUS AND EXPERIMENTAL PROCEDURE	31
A. Introduction.	31
B. Apparatus	32
C. Experimental Procedure	52
IV. DATA REDUCTION AND ANALYSIS	59
A. The Continuum Signal	59
B. The Visible Scan Data	60
C. The VUV Scan Data	63
V. RESULTS AND DISCUSSION	66
A. Results and Error Estimates	66
B. Conclusions.	69
C. Future Experiments	70
BIBLIOGRAPHY	71

profiles and the modifications made by Mr. Louis Palumbo to the program written by Mr. Warden.

I am greatly appreciative of the efforts of Mr. Stanley Wexler of Arnold Ratner Associates, Inc., who demonstrated the qualities of the Baratron capacitance manometer so necessary for the successful completion of this experiment and provided me with the use of this instrument for such a generous period of time.

CHAPTER I
INTRODUCTION

A. Preliminary Discussion

The experimental widths of ion spectral lines are of interest since application of certain classical approximations¹, valid in the case of neutrals, are of questionable validity in the case of ions due to acceleration of the perturbing electrons in the field of the ion^{2-5, 69}. Measurements of the widths of isolated ion lines have been carried out previously in plasmas⁶⁻¹⁵ for which the electron thermal energy kT is greater than, or of the order of the energy difference ΔE between one of the energy levels of the transition and the nearest perturbing level. Broadening collisions by electrons with thermal energies in this range are predominantly inelastic; and cross sections and collision rates are readily estimated by quasiclassical methods^{5, 16}.

Under the conditions of the experiment to be described here the electron thermal energy is much less than threshold (ΔE) and the broadening is due predominantly to elastic collisions (with possible superelastic and higher multipole inelastic contributions). Since no (necessarily quantum mechanical) calculations from first principles of the electron impact broadening have been carried out for

NOTE: This report in dissertation form was previously submitted to the Faculty of the Graduate School of the University of Maryland in partial fulfillment of the requirements for the degree of Doctor of Philosophy, 1969.

this case, the measured broadening is compared to an extrapolation of the quasiclassical inelastic case to below threshold⁵. This extension of the quasiclassical inelastic cross sections below threshold is indicated^{17,68} from the calculated values just above threshold.

For the purpose of comparison, a computer plots the (optically thick) theoretical profiles of the resonance multiplets as calculated from the effective absorption coefficient, using the extrapolated quasiclassical estimate for the electron broadening. The computer plots are compared to the photoelectric experimental scan of the multiplet for the independently measured plasma conditions of electron temperature, density and atomic concentration.

The resonance multiplets of N II and C II were chosen for study because of their large threshold energy (~ 10 eV) values compared to kT (~ 2 eV) and accurately known oscillator strengths^{18,19,65}. The low first ionization potentials of these elements make them well suited for study at the low temperatures required for a critical test of the theory.

The measurements of the profiles of the resonance multiplets, which occur in the vacuum ultraviolet (VUV) region of the spectrum, were obtained by observing the radiation produced by reflecting the shock wave generated by a T-type electromagnetic shock tube^{20,21}. A 4 KJ electrical discharge into 40 torr of helium, to which the test elements (and hydrogen) were added, produced in the shocked plasma an electron density of $(3.3 \pm 0.3)10^{17}$ cm^{-3} as obtained

from the halfwidth of the He I 3889 Å line, and an electron temperature of $(19.0 \pm 0.6)10^3$ °K as obtained from the ratio of the total intensities of the He I 4713 Å and H β 4861 Å lines. The addition of 1.0 percent of hydrogen gas was found necessary to minimize the ionization relaxation time behind the shock front^{22,23}. The experimental results indicate agreements with theoretical line shapes computed using widths which are 1.5 times the nominal theoretical width (of expected precision X2) for N II and equal to the nominal theoretical width for C II.

Chapter I continues with a brief review of the semiempirical approximation used for isolated ion lines. The purpose of the experiment is described in more detail in the light of the theory and the validity of applying the theoretical approximations to this plasma examined. In Chapter II the spectroscopic theory applied to line intensities to obtain temperature and line profiles is presented, and the question of the plasma equilibrium is discussed. Chapter III describes the experiment from the point of view of equipment requirements, in detail, and ends with a description of the experimental procedure. Chapter IV includes the reduction and analysis of the data and the required corrections. Finally, Chapter V presents the results, discussion and conclusions.

B. Survey of Recent Theory and Experiments

The study of spectral line shapes in plasmas is motivated by the information disclosed regarding the physical properties of the plasma. The line shape provides a nonperturbing probe of the plasma that may reveal the physical state of a source as convenient as the laboratory or as remote as a star.

The two principal types of broadening in addition to natural broadening are Doppler and pressure broadening. Doppler broadening dominates at relatively high temperatures and low densities and serves as an ion temperature probe for such plasmas, while pressure broadening dominates at relatively high densities and low temperatures and consequently serves as a density probe for these plasmas. Pressure broadening includes Stark, resonance and Van der Waals broadening but Stark broadening dominates when the plasma is more than one percent ionized. General reviews of line broadening theory are provided by Unsöld,²⁴ Breene,²⁵ Traving,²⁶ Ch'en and Takeo.²⁷ An early review of the special case of pressure broadening by electrons and ions (prior to recent development of the quantum impact theory) is provided by Margenau and Lewis.²⁸ More recent developments are presented in References 1,5,29-36,44.

The pressure broadening³² may be classified into two extremes of approximation, the quasistatic approximation and the impact approximation. With $\Delta\omega$ the angular

frequency separation of the emission from the line center and τ_c the collision duration (in seconds) between emitter and perturber, then the quasistatic approximation applies for conditions $\Delta\omega \tau_c \gg 1$ while the impact approximation applies for conditions $\Delta\omega \tau_c \ll 1$.

Since ions are much more slowly moving than the electrons, τ_c (ion) $\gg \tau_c$ (electron), and thus the impact approximation will be applied to both electrons and ions very near the line center, the quasistatic approximation applied to ions and the impact approximation to electrons over some intermediate region of the line shape, and the quasistatic approximation applied to both ions and electrons far enough out on the wings.

The impact approximation is valid when times $1/\omega$ between collisions substantially exceed the calculation time of the approximation, namely the range Δt of the time variable in the Fourier transform of the line shape, which in turn must be substantially larger than the duration of a single collision τ_c as defined in Eq. (14). Thus the impact approximation is valid if (in the one-electron approximation)

$$1/\omega \gg \Delta t \gg \tau_c \quad (1)$$

The impact theory often utilizes the classical path approximation which permits averaging the perturbations over the perturber trajectories which are assumed to be the straight paths (in the case of neutral atoms) or hyperbolic paths (in the case of ions) of classical point charges. The parameters of the perturber paths are the

perturber impact parameter, ρ , and the perturber velocity, v . The validity criterion for this classical path approximation, where λ is the perturber deBroglie wavelength, is

$$\rho \gg \lambda . \quad (2)$$

The adiabatic condition,³² valid in the case of neutrals, is expressed by the inequality $kT \gg \Delta E$ where ΔE is the separation of the perturbed from the perturbing level. That is, the transfer of energy from the perturber to the emitter must be a small fraction of the perturber kinetic energy. This insures that the energy (velocity) distribution of the perturbers over which the individual perturbations are eventually averaged will not be altered significantly by reaction with the emitter. This condition is somewhat severe since the emission is the quantity to be observed rather than alterations in the perturber distribution insufficient to affect substantially the calculation of the emission. The adiabatic condition becomes invalid^{5, 69} in the consideration of broadening of ion lines by electrons due to the acceleration of the electrons in the Coulomb field of the ion, inelastic cross-sections peaking at low incident energies here.

The most common approach is to use the quasistatic approximation for the broadening due to the ions and the impact approximation for the broadening due to the electrons. The emitter is considered with its energy levels shifted in the static electric field of a given arrangement of static ions. The electron impact broadening calculation is then performed and the result averaged over a distribution of electric fields,

each corresponding to a different arrangement of static ions. If the condition that the ions do not move during the time between electron collisions with the emitter is not fulfilled, the impact approximation for ions must be used.

The line shape is given in the impact approximation for electrons and the quasistatic approximation for ions as ^{1,37}

$$I(\omega) = \frac{1}{\pi} \int dF W(F) \text{Re} \sum_{i' r f f'} \langle i | \mu_r | f \rangle \langle i' | \mu_r | f' \rangle \times \langle \langle i f | [i \omega - \omega_{if}(F)] - \phi_{if}(F)]^{-1} | i' f' \rangle \rangle \quad (3)$$

where $W(F)$ is the distribution of ion field strengths F , $\omega_{if}(F)$ is the unperturbed line position in the ion field F , $\phi_{if}(F)$ is the impact broadening (relaxation) operator. The energy levels perturbing level i are denoted i' and the energy levels perturbing level f are denoted f' . The μ_r are the (dimensionless) dipole operator components. All the information regarding electron impact broadening and shift is contained in ϕ_{if} which includes the average over electron velocities and impact parameters.

Line width calculations for certain neutral helium ³⁵ lines for which wavefunctions are well known and deviations from adiabaticity are accounted for and for which the lines are isolated (the separation of perturbed and perturbing energy levels exceeds the line width) gave agreement with measurements to better than 20 percent. ^{38,67} Extending these

calculations to the broadening of isolated lines of heavier elements³⁶ for which Coulomb approximation wavefunctions and L-S coupling were assumed nevertheless resulted in comparable agreement with experiment.^{38, 68} As for neutral helium, the line shape is Lorentzian with the width w and shift d given by

$$w + id = - \langle if | \phi_{if} | if \rangle \quad (4)$$

and the ion field dependence of ϕ_{if} can be neglected so that calculation of ϕ_{if} is equivalent to calculating the classical S matrix averaged over perturber impact parameters, velocities and directions.

When the isolated neutral line approximations were extended to heavy isolated ion lines and the assumptions of hyperbolic trajectories⁴⁴ and additional strong collision terms included, calculated widths⁵ agreed with measured widths⁶⁻¹⁵ for $kT \gg \Delta E$. For $kT \ll \Delta E$ the quasiclassical inelastic cross section makes a vanishing contribution to the observed broadening which may then be due to superelastic collisions and inelastic collisions involving higher multipole interactions as well as elastic collisions. As an estimate, the quasiclassical inelastic cross section is therefore extrapolated in the Boltzmann average to zero perturber energy to account for the observed broadening.

When the widths of the 45 isolated ion lines above were calculated⁵ using this extrapolation (the semiempirical approximation, see Section C), agreement to a factor of 1.5

was found with the experimental widths which represented values of $kT/\Delta E$ from 0.5 to 50 (Fig. 1). A factor of 1.5 error was expected in the estimate of the Gaunt factor used in this extrapolation.

C. The Semiempirical Approximation

Griem has proposed an application of Baranger's^{31, 32} expression for the line width

$$w_{if} = \frac{1}{2} N_e \left\{ \nu \left[\sum_{i'} \sigma_{i'i} + \sum_{f'} \sigma_{f'f} + \int |f_i(\theta, \phi) - f_f(\theta, \phi)|^2 d\Omega \right] \right\}_{av} \quad (5)$$

to the electron impact broadening of lines for which the perturbing collisions are predominantly elastic, but without directly computing the elastic term of Baranger's expression. Instead, the inelastic terms are computed by the Bethe-Born approximation, and, with the proper choice of a Gaunt factor, the average over perturber velocities is carried below the inelastic threshold limit to zero energy. In the above expression w_{if} is the line halfwidth at half maximum in rad/sec, N_e the electron density in cm^{-3} , ν the relative perturber velocity in cm/sec, i and f indicate the unperturbed initial and final states, respectively, of the observed transition, $\sigma_{i'i}$ is the inelastic cross section in cm^2 for a collisional transition from the unperturbed initial energy level (i) to a perturbing level (i'), $\sigma_{f'f}$ is the similar cross section for the final unperturbed energy level (f), $f_i(\theta, \phi)$ and $f_f(\theta, \phi)$ are the elastic scattering amplitudes, in centimeters,

of the initial and final states, respectively, $d\Omega$ is the element of the solid angle, and $\{ \}_{av}$ denotes the (Boltzmann) average over perturber (electron) velocities.

The line width from Eq. (4) is compared to the Baranger expression in the following way. The width is expressed in the classical path approximation in terms of the classical path S matrix³⁵

$$\begin{aligned} w_{if} &= -\text{Re} \langle if | \phi_{if} | if \rangle \\ &= N_e \left\{ 2\pi\nu \int \rho d\rho \langle if | 1 - S_i S_f^* | if \rangle \right\}_{av} \end{aligned} \quad (6)$$

where $(*)$ means complex conjugate. Expanding the S matrices S_i and S_f for the initial and final states i and f in a Dyson series and using a dipole-monopole interaction potential eventually yields

$$\begin{aligned} w_{if} &= \frac{1}{2} N_e \left\{ 2\pi\nu \int_0^\infty \rho d\rho (1/\hbar^2) \sum_{i'f'} \left[\left| \langle i | \int_{-\infty}^{\infty} dt V(t) | i' \rangle \right|^2 \right. \right. \\ &\quad \left. \left. + \left| \langle f | \int_{-\infty}^{\infty} dt V(t) | f' \rangle \right|^2 \right] \right\}_{av}. \end{aligned} \quad (7)$$

where \hbar is Planck's constant, $V(t) = -Ze^2 \underline{r} \cdot \underline{r}(t) / |\underline{r}(t)|^3$ is the dipole-monopole interaction potential, e is the electronic charge, \underline{r} is the optical electron coordinate vector and $\underline{r}(t)$ is the perturbing electron coordinate vector.

Seaton³⁹ gives the following quasiclassical inelastic cross section from the Bethe-Born approximation, where $P_{i'i}$ is the probability of a transition occurring at ρ , as

$$\begin{aligned}\sigma_{i'i} &\approx 2\pi \int_0^{\infty} \bar{P}_{i'i} \rho dp \\ &\approx 2\pi \int_0^{\infty} (1/\hbar^2) |\langle i' | \int_{-\infty}^{\infty} dt V(t) | i \rangle|^2 \rho dp\end{aligned}\quad (8)$$

from which the Baranger expression Eq. (5) for the width immediately follows if the elastic scattering amplitudes are omitted but the thermal average over velocities is extended to zero velocity.

Bethe⁴⁰ obtains from the Born approximation

$$\sigma_{i'i} = \frac{8\pi^2}{3^{3/2}} \frac{E_H}{kT} |\langle i' | r | i \rangle|^2 g_{qc}\quad (9)$$

for the inelastic cross section for $kT \gg \Delta E$, where E_H is the ionization potential of hydrogen. Evaluating Seaton's expression for $\sigma_{i'i}$ with classical limits on the impact parameter yields the quasiclassical Gaunt factor

$$g_{qc}^5$$

Seaton¹⁶ and Van Regemorter⁴¹ have proposed a semi-empirical effective Gaunt factor which agrees well in the range of high electron energies with the Gaunt factors obtained from quasiclassical considerations in determining the inelastic cross section (Fig. 2 of Ref (5)). Here the Bethe-Born approximation represents the proper limit for allowed dipole transitions. At low electron energies the semiempirical Gaunt factor approaches a constant 0.2 which agrees with the quasiclassical threshold ($kT = \Delta E$)

Gaunt factor to within a factor of 1.5 for electron energies within 3 eV of the transition energy.⁵ The semiempirical Gaunt factor has the further property that it is independent of both the Coulomb parameter $ze^2/\hbar v$ (z is the effective nuclear charge, e. g., $z = 1$ for singly ionized atoms) and the quantity $2n^2/1+z$ where n is the effective principal quantum number of the unperturbed level defined in Eq. (13). This Gaunt factor is assumed to have the same value (0.2) below threshold, where quasiclassical estimates of Gaunt factors cannot be made since there exists no classical analogue. Thus, as Griem⁵ points out, the extrapolation of the semiempirical Gaunt factor may account for the first truly quantum mechanical effect in electron impact broadening.

For electron energies well below threshold the quantum mechanical or elastic process dominates. Consider the contribution to the line width of the perturbation of only a single level. For a Maxwellian distribution of electron velocities and letting $g(-)$ and $g(+)(kT)$ be the Gaunt factors below threshold and above threshold, respectively, and following Griem,⁵

$$\begin{aligned}
 W_{ii} &\approx \frac{4\pi^2}{3^{3/2}} N_e E_H |\langle i' | \mathcal{L} | i \rangle|^2 \left\{ g(-) \int_0^{(2\Delta E/m)^{1/2}} \frac{v^3}{E} \exp(-E/kT) dv \right. \\
 &\quad \left. + g(+)(kT) \int_{(2\Delta E/m)^{1/2}}^{\infty} \frac{v^3}{E} \exp(-E/kT) dv \right\} / \int_0^{\infty} v^2 \exp(-E/kT) dv \\
 &\approx 8(\pi/3)^{3/2} N_e (\hbar/m a_0) (E_H/kT)^{1/2} |\langle i' | \mathcal{L} | i \rangle|^2 \\
 &\quad \times \left\{ [g(+)(kT) - g(-)] \exp(-\Delta E/kT) + g(-) \right\}, \quad (10)
 \end{aligned}$$

where a_0 is the Bohr radius, m is the electron mass and $E = \frac{1}{2}mv^2$. Here $g_{(+)}(kT)$ is considered to vary slowly over the velocity distribution and may be either the Seaton-Van Regemorter semiempirical Gaunt factor or a quasiclassical Gaunt factor. $g_{(-)}$ is the semiempirical Gaunt factor extrapolated below threshold. Eq. (10) indicates the dominance of the inelastic contribution (with Gaunt factor $g_{(+)}(kT)$) for $kT \gg \Delta E$ and its exponentially diminishing contribution as kT approaches threshold ΔE (the curved plot in Figure 1). Below threshold the elastic contribution (with Gaunt factor $g_{(-)}$) dominates as seen in Figure 1.

The semiempirical line width for the ion lines of this experiment ($kT \ll \Delta E$) becomes [from Eq. (10) with $g_{(-)} = 0.2$]:

$$\begin{aligned}
 W_{calc} &= \sum_{i \neq f} (W_{i \rightarrow i} + W_{f \rightarrow f}) \\
 &= 8(\pi/3)^{3/2} N_e (\hbar/m a_0) (E_H/kT)^{1/2} (0.2) \\
 &\quad \times (\langle i | r^2 | i \rangle + \langle f | r^2 | f \rangle) \quad (\text{rad/sec}) \quad (11)
 \end{aligned}$$

The matrix elements of r^2 are approximated by the hydrogenic ion relation

$$\langle i | r^2 | i \rangle = \frac{n_i^2}{2(z+1)^2} [5n_i^2 + 1 - 3l_i(l_i+1)] a_0^2, \quad (12)$$

and the effective principal quantum number n_i by

$$n_i^2 = (z+1)^2 E_H / (E_\infty - E_i) \quad (13)$$

Here l_i is the initial orbital quantum number for the electron undergoing transition, E_∞ is the ionization energy of the test ion and E_i is the energy of the initial state.

D. Purpose of the Experiment

It is the purpose of this experiment to measure the profiles of the N II and C II resonance lines and to compare them with computed profiles corresponding to values of w_{calc} as obtained from Eq. (11) for the experimental conditions of $T = 19000$ °K and $N_e = 3.3 \times 10^{17} \text{ cm}^{-3}$.

The energy levels for the N II resonance transitions ($\lambda = 1085.1 \text{ \AA}$) relevant to the calculation are $2s^2 2p^2(^3P)$ at 89.3 cm^{-1} (0.011 eV), $2s2p^3(^3D^0)$ at 92245 cm^{-1} (11.4 eV), and $2s^2 2p(^2P^0)3p(^3D)$ at 166616 cm^{-1} (20.6 eV).¹⁸ The first and second levels comprise the transition. The second level is also the nearest perturbing (by dipole interaction) level to the first and the third level is the nearest perturbing level to the second. Thus for N II, $\Delta E_i \geq 9.20 \text{ eV}$ and $\Delta E_f \geq 11.39 \text{ eV}$. For C II (at $\lambda = 1335.3 \text{ \AA}$) the relevant levels are $2s^2 2p(^2P^0)$ at 43 cm^{-1} (0.0053 eV), $2s2p^2(^2D)$ at 74932 cm^{-1} (9.28 eV), and $2p^3(^2D^0)$ at 150465 cm^{-1} (18.6 eV).¹⁸ For C II, $\Delta E_i \geq 9.27 \text{ eV}$ and $\Delta E_f \geq 9.27 \text{ eV}$.

The presently deduced values of $w_{\text{exp.}} / w_{\text{calc}}$ for N II and C II (w_{exp} being the experimentally deduced width) are seen to lie at $kT/\Delta E \approx 0.18$ on the abscissa of Figure 1. Here the ratio of the elastic (plus superelastic) broadening

to inelastic broadening is $\sim 250/1$, and thus determined values of $w_{\text{exp}}/w_{\text{calc}}$ of order of unity would strongly support the semiempirical approach.

The calculated widths of N II 1085 Å and C II 1335 Å are 6×10^{10} rad/sec (0.0038 Å) and 10×10^{10} rad/sec (0.0088 Å) respectively, much smaller than the resolution (0.14 Å) of the spectrograph used. The lines were therefore made optically thick so that good signal was obtained on the optically thin wings and compared to the profiles²² computed using the values of w_{calc} above. The computed profiles agreed on the optically thin wings within a factor-of-two with the experimental profiles.

E. Validity of the Approximations

To ascertain whether the plasma and atomic parameters justify the application of the impact approximation and/or the classical path approximation for the electrons, and the quasistatic approximation for ions, the validity criteria of Sect. B for these approximations must be tested.

The collision duration τ_c for electrons may be estimated by

$$\tau_c = \rho_0 / v \quad (14)$$

where v is the relative velocity between the perturbing electron and the emitter (hereafter the velocity) and ρ_0 , the "optical radius," is given by

$$w = \pi \rho_0^2 v N_e \quad (15)$$

where w (rad/sec) is the electron collision frequency (estimated by the line width) and N_e is the electron

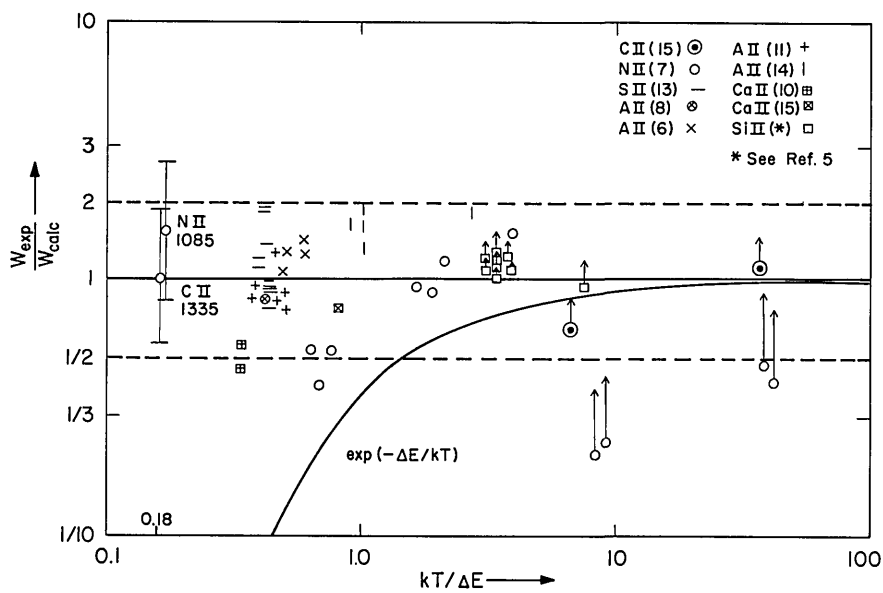


Fig. 1 - Comparison with the semiempirical width. (See Ref. 66.)

number density. The atomic parameters of N II and the plasma parameters of electron temperature and density yield $w_{\text{calc}} = 6 \times 10^{10}$ rad/sec, $\rho_0 = 2.4 \text{ \AA}$, and $v = 10^8$ cm/sec. Thus from Eq. (1),

$$1/w = 10^{-11} \gg \Delta t \gg \tau_c = 2.4 \times 10^{-16} \text{ sec.} \quad (16)$$

and the criterion for the impact approximation Eq. (1) for electrons is well satisfied, and holds for about $7 \times 10^3 w$ (about 21 \AA) onto the wings (where $\Delta\omega\tau_c \ll 1$).

The quasistatic approximation for the ions requires that

$$v_i / w \ll \rho_m \quad (17)$$

where the relative velocity of the ion is v_i , the time between electron collisions is $1/w$, and the mean distance between ions is ρ_m . Stated another way, $\sigma \equiv \rho_m w / v_i \gg 1$. For this plasma $\sigma \approx 0.05$, and the quasistatic approximation for ions seems not valid. However, the impact approximation for ions only applies out to $\Delta\omega \rho_m / v_i \approx 1$, i.e., to about $20 w \approx 0.06 \text{ \AA}$ on the wings while, due to the plasma conditions, the line does not become optically thin until about twice this distance from the line center. Since ion effects on isolated ion lines are small in any case (any small effect on the halfwidth being largely cancelled by Debye shielding¹), with possible exception of a contribution to asymmetry in the far wings (discussed in Chapter V), the ion contribution to the line broadening will not be considered further.

The criterion for treating the electron perturbers as classical point charges is marginally satisfied, i.e., $\lambda \approx 1 \text{ \AA}$ while $\rho_0 \approx 2.3 \text{ \AA}$. Since the only available theory for comparison with experiment is the semiempirical approximation that does not in fact utilize the classical path approximation, this point is only noted.

CHAPTER II

DIAGNOSTIC THEORY

A. Spectroscopic Theory

The plasma under study will be regarded to be in LTE and therefore scattering of radiation can be neglected and the equation of radiative transfer written¹

$$\frac{d I(\omega, x)}{dx} = \epsilon(\omega, x) - [\kappa(\omega, x) - \epsilon'(\omega, x)] I(\omega, x) \quad (18)$$

where $I(\omega, x)$ is the specific intensity of the radiation field or power per unit area per solid angle per angular frequency interval, $\epsilon(\omega, x)$ is the emission coefficient for spontaneous transitions or power per unit volume per solid angle per angular frequency interval, $\kappa(\omega, x)$ is the absorption coefficient and $\epsilon'(\omega, x)$ is the negative absorption coefficient for stimulated emission. Equation (18) expresses the net gain or loss of radiant intensity with position in the plasma due to the internal radiative and absorption processes (which depend on the radiation field intensity) and to the spontaneous emission (which does not). Writing the competing coefficients of the radiation $I(\omega, x)$ as the effective absorption coefficient

$$\kappa'(\omega, x) \equiv \kappa(\omega, x) - \epsilon'(\omega, x) \quad (19)$$

and considering for the moment the case where radiative and absorption processes balance, i.e., $\frac{dI}{dx} = 0$, then

$$\epsilon(\omega) = \kappa'(\omega) I(\omega) \quad (\text{Kirchoff's Law}) \quad (20)$$

where $I(\omega)$ is now the equilibrium intensity (source function) or, for LTE, the blackbody intensity $B(\omega, T)$ and T is the equilibrium temperature. Thus for LTE

$$B(\omega, T) = \epsilon(\omega, T) / \kappa'(\omega, T) \quad (21)$$

The equation of radiative transfer (18) is easily integrated when ϵ and κ' are independent of position as in a uniform plasma to yield

$$I(\omega, d, T) = B(\omega, T) \{1 - \exp[-\kappa'(\omega, T)d]\} \quad (22)$$

where $I(\omega, 0, T) \equiv 0$ and d is the geometric depth of the plasma.

The effective absorption coefficient is expressed (e.g., Ref. (1), Chapter 7)

$$\kappa'(\omega, T) = 2\pi^2 r_0^2 c f_{mn} N_n [1 - \exp(-\hbar\omega/kT)] L(\omega) \text{ cm}^{-1} \quad (23)$$

for transitions between lower state n (statistical weight g_n and population N_n) and upper state m (statistical

weight g_m and population N_m) where f_{mn} is the absorption oscillator strength and the energy difference between states m and n is $\hbar\omega$ and the LTE relation

$$N_m/N_n = (g_m/g_n) \exp(-\hbar\omega/kT) \quad \text{has been used.}$$

Here $L(\omega)$ is the line shape with the normalization

$$\int L(\omega) d\omega = 1. \quad \text{The constant } r_0 \text{ is the classical}$$

electron radius, c is the speed of light and k is

Boltzmann's constant.

For an optically thin line ($I \ll B$) the expression Eq. (22) for $I(\omega, d, T)$ becomes

$$I(\omega, d, T) = B(\omega, T) n'(\omega, T) d. \quad (24)$$

The blackbody expression

$$B(\omega, T) = \frac{\hbar\omega^3}{4\pi^3 c^2} \exp(-\hbar\omega/kT) [1 - \exp(-\hbar\omega/kT)]^{-1} \quad (25)$$

and Eq. (23) then give

$$I(\omega, T) = \frac{\hbar\omega^3 r_0 d}{2\pi c} f_{mn} N_n L(\omega) \exp(-\hbar\omega/kT). \quad (26)$$

Integrating over wavelength assuming that $\omega^3 \exp(-\hbar\omega/kT)$ varies slowly over the range where $L(\omega)$ contributes leads to

$$I(T) = \frac{\hbar\omega^3 r_0 d}{2\pi c} f_{mn} \frac{g_n^0}{Z^0} N^T (1-\alpha) \exp(-E_m/kT) \quad (27)$$

where $N_n = \frac{g_n^0}{Z^0} N^0 \exp(-E_n/kT)$, $N^T(1-\alpha) = N^0$,

$$\omega \equiv \omega_{mn} = (E_m - E_n)/h,$$

and E_m and E_n are the energies of the states m and n , respectively, measured from the ground state. For the single chemical species considered, g_n^0 is the statistical weight of the n th state of the neutral atom, N^0 is the neutral density, Z^0 the neutral partition function, N^T the total number density of atoms and ions and α is the fractional ionization and depends on the electron density and temperature through the Saha relation

$$1 - \alpha = 1 / \{ [S(T)/N_e] + 1 \} \quad (28)$$

where $S(T)$ is the Saha function^{1, 42} which, with partition functions, has been conveniently tabulated for a wide range of temperatures and electron densities⁴³.

For the present experiment the ratio of total line intensities for two neutral species (1) and (2) is useful. This is, from Eq. (27),

$$\frac{I^{(1)}(T)}{I^{(2)}(T)} = \left(\frac{\lambda^{(2)}}{\lambda^{(1)}} \right)^3 \frac{f_{mn}^{(1)}}{f_{mn}^{(2)}} \left(\frac{g_m^0}{Z^0} \right)^{(1)} \left(\frac{g_n^0}{g_n^0} \right)^{(2)} \frac{(N^T)^{(1)}}{(N^T)^{(2)}} \frac{1 - \alpha^{(1)}}{1 - \alpha^{(2)}} \exp \left[\frac{(E_m^{(2)} - E_m^{(1)})}{kT} \right] \quad (29)$$

where the atomic mix ratio is given by $(N^T)^{(1)} / (N^T)^{(2)}$

The ratio of total line intensities is particularly sensitive to temperature if the transitions are such

that $(E_m^{(2)} - E_m^{(1)}) \gg kT$, The relative change in $I_{HeI\ 4713} / I_{H\beta\ 4861}$ at 19000 °K is 13.5 times the relative temperature change.

For the optically thick ion resonance lines, $\kappa'(\omega)d$ is large, and for the purpose of calculating the line profile

$$I(\omega, T) / B(\omega, T) = 1 - \exp(-\kappa'(\omega, T)d) \quad (30)$$

is a convenient form of Eq. (22). For $\hbar\omega \gg kT$, and using a Lorentz shape for the line profile (since the isolated ion lines are of concern here),

$$L(\omega) = \left\{ \pi w \left[1 + \left(\frac{\omega - \omega_0}{w} \right)^2 \right] \right\}^{-1} \quad (31)$$

one finds

$$\kappa'(\omega, T) = 2\pi r_0 c f_{mn} N_m / w \left[1 + \left(\frac{\omega - \omega_0}{w} \right)^2 \right] \quad (32)$$

or

$$\kappa'(\lambda, T) = \lambda_0^2 r_0 f_{mn} N_m / w_\lambda \left[1 + \left(\frac{\lambda - \lambda_0}{w_\lambda} \right)^2 \right] \times 10^{-8} \text{ cm}^{-1} \quad (33)$$

$$\approx \lambda_0^2 w_\lambda r_0 f_{mn} N_m / (\lambda - \lambda_0)^2 \times 10^{-8} \text{ cm}^{-1} \quad (34)$$

on the far wings. Here w, ω and ω_0 are the half halfwidth of the line, frequency of radiation, and the line center in radians per second, while w_λ, λ and λ_0 are the corresponding quantities in Angstroms.

The ground state population of the nitrogen ion resonance line is given by

$$N_m \equiv N_i^+ = \frac{g_i^+ N^+}{Z^+}, \text{ since } E_i^+ \approx 0, \quad (35)$$

N^+ is the ion density of the same chemical species as N_i^+ , g_i^+ the statistical weight of the ion ground state, Z^+ the partition function of the ion and E_i^+ the ion ground state energy.

The nitrogen ion density, N_N^+ , for example, is found from the quasineutrality condition

$$N_e = N_H^+ + N_{He}^+ + N_N^+ \quad (36)$$

and the measured mix ratios N_H^T/N_N^T and N_{He}^T/N_N^T

The expression Eq. (30), where $\kappa'(\lambda, T)$ is expressed by Eq. (33) summed over the members of the multiplet, is folded with a triangular instrument profile (Eq. (48)) and compared to the experimental data in Figs. 7 and 8

B. LTE and Rankine-Hugoniot Comparison

In order to calculate the theoretical width of the line observed the electron density and electron temperature of the plasma in which the line is produced must be known (see Chapter I).

The electron density may be obtained from the line width at half maximum intensity for a neutral line such as He I 3889 Å to which line broadening theory⁴⁴ may be applied with confidence.

The temperature may be obtained from the ratio of total line intensities for two spectral lines (see Eq. (29)). For this method to be valid, the upper energy states of the two transitions must be populated in the ratio predicted for LTE plasmas by a Boltzmann distribution at the electron temperature. Deviations from Boltzmann equilibrium may occur due to radiative decay competing with the collisional depopulation rate, or to failure of the thermalized electrons to establish collisional equilibrium of the atomic states at the electron temperature by the time the plasma is observed. Temperature and density inhomogeneities may be sufficient to cause error in the interpretation of data, while the optical depth of the plasma may have to be taken into account in determining the line intensities. Each of these conditions must be checked individually to assess the validity of the interpretation of observations of the plasma with respect to plasma density and temperature.

The two lines used here for the temperature determination are H β at 4861 Å and He I at 4713 Å. Griem^{1,45} gives a criterion for the existence of LTE for states with principal quantum number n and higher for a time-independent and homogeneous plasma as

$$N_e \geq 7 \times 10^{18} \frac{(Z+1)^7}{n^{17/2}} \left(\frac{kT}{E_\infty} \right)^{1/2} \text{ cm}^{-3} \quad (37)$$

where N_e and T are the electron density and temperature, respectively, E_∞ is the ionization energy of the atom or ion and $Z=0$ for neutrals, etc. This formula states that the collisional depopulation rate of the state n must be at least ten times its radiative decay rate for its population to be within ten percent of that calculated from states $m > n$ using the Boltzmann factors and the electron temperature.⁴⁶ Further, if this criterion is satisfied for at least one level below the reduced ionization limit, the free electrons may be assumed to have a thermal velocity distribution. The helium and hydrogen neutral atoms of the present plasma satisfy by more than an order of magnitude this criterion for the lower ($n = 2$) states of the transitions of concern at the conditions of this experiment, i.e., $N_e = 3.3 \times 10^{17} \text{cm}^{-3}$ and $kT = 1.64 \text{ eV}$. This suggests an existence of LTE to ~ 1 percent,⁴⁷ subject to spatial and time-dependent requirements yet to be considered.

The VUV lines investigated are the N II and C II resonance lines, and LTE must therefore be established between the ground state of this ion and the first excited state in order to validate the expression (Eq. (33)) for the effective absorption coefficient upon which the line shape depends. Here the collisional population rate of the ground state must be at least ten times the radiative population rate from the first excited level. If the line is optically thick (the optical depth for

N II 1085 Å line is $\sim 5 \times 10^8$ for the experimental conditions), the radiation field is in equilibrium at the electron temperature and the populations of the ground and first excited states are not changed by radiative transitions between them. Overpopulation will then occur by radiative transitions from excited states higher than the first to the ground state, but since this rate is usually a factor of ten smaller than the spontaneous decay rate from the first excited state, the criterion may be relaxed to requiring the collisional population rate of the ground state to be of the same order as radiative depopulating rates (were the plasma thin) of the first excited state. Thus results the requirement^{1,45}

$$N_e \geq 10^{17} (Z+1)^7 \left(\frac{kT}{E_\infty} \right)^{1/2} \left(\frac{E_2 - E_1}{E_\infty} \right)^3 \text{ cm}^{-3} \quad (38)$$

for LTE between the ground state (E_1) and the first excited state (E_2) which is satisfied for the nitrogen ion by a factor of two (LTE between E_2 and higher states is insured by the above criterion in the optically thick case since it is not depopulated by the resonance transition due to trapping).

The radiation from the plasma generated by the present shock tube rises to maximum intensity in about 3 μ sec or, as will be seen, about ten excitation-ionization relaxation times. The establishment of excitation and ionization equilibrium is therefore through a series of near LTE quasistationary excited states.^{1,45} The plasma decays in

about 8 μsec . Thus the plasma event lasts for about 10 μsec , which is about three to ten times that of other electromagnetic shock tube plasmas.^{22,48-55} The characteristic excitation-ionization time τ_1 is of the order of the reciprocal of the collisional excitation rate of the first excited level times the fraction of eventual ions.^{1,45}

$$\tau_1 \approx \frac{1.15 \times 10^7 (Z+1)^3 N^+}{f_{21} N_e (N^+ + N)} \left(\frac{E_2 - E_1}{E_\infty} \right) \left(\frac{kT}{E_\infty} \right)^{1/2} \exp \left(\frac{E_2 - E_1}{kT} \right) \text{ sec.} \quad (39)$$

Here N^+ is the degree of ionization of the species, E_2 and E_1 are ground state and first excited state energies respectively. For neutral helium, $\tau_1 \approx 0.3 \mu\text{sec}$ so that thirteen relaxation times pass between shock arrival and the observation time. This value of τ_1 may be somewhat pessimistic due to neglect of substantial preexcitation and slight ionization by the incident shock which passes the observation point 0.6 μsec earlier than the reflected shock arrival.

The excitation-ionization times for neutral hydrogen and neutral nitrogen are about $10^{-2} \mu\text{sec}$. Equilibration of $n = 2$ with higher levels in hydrogen and helium requires about $10^{-5} \mu\text{sec}$ and the excitation of the nitrogen ion about $10^{-4} \mu\text{sec}$.

In the decaying plasma the criterion for validity for LTE in a transient plasma, assuming the temperature drops completely, which it does not, in 10 μsec , becomes

$$\left| \frac{T(t + \tau_1) - T(t)}{T(t)} \right| \approx .03 \ll 1 \quad (40)$$

During the equilibrium relaxation time τ_1 , the plasma atoms diffuse a distance δ given by ^{1,45}

$$\delta \approx v \tau \left(\frac{\tau_1}{\tau}\right)^{1/2} = \frac{7 \times 10^{14}}{A^{1/4}} \left(\frac{kT}{E_H}\right)^{1/2} \left(\frac{E_2 - E_1}{f_{21} E_H}\right)^{1/2} \frac{\exp[(E_2 - E_1)/kT]}{[(N+10N^+)(N+N^+)]^{1/2}} \quad \text{cm} \quad (41)$$

where v is the thermal velocity of the atoms (ions),

τ is the mean time between elastic or charge-exchange collisions, $(\tau_1/\tau)^{1/2}$ is the "random walk" factor, E_H is the ionization potential of hydrogen, and A is the atomic weight of the gas atoms. For this plasma

$\delta \approx 0.02$ cm for the distance an atom or ion diffuses before it reaches thermal equilibrium with its neighbors.

The greatest spatial change in the plasma temperature takes place near the shock tube walls over a radial distance given approximately by $\delta \tau_0/\tau_1$, where τ_0 is the time of observation after shock arrival (4 μsec), in this case 13 times τ_1 . Thus the plasma temperature varies by ~ 8 percent over a single equilibration distance and may be regarded as being close to local LTE throughout the boundary layer. The time τ_0 is greater than the time needed to establish pressure equilibrium (at a sound speed of 1.0 cm/ μsec , tube radius 1.25 cm). Assuming a linear temperature rise in the plasma from 300 $^\circ\text{K}$ at the tube wall to the spectroscopic temperature of 19,000 $^\circ\text{K}$ at 13 times δ or 0.26 cm from the tube wall implies an average heavy particle density in the boundary region

of $1.9 \times 10^{19} \text{ cm}^{-3}$ to be consistent with the observed electron density of $3.3 \times 10^{17} \text{ cm}^{-3}$ (or $0.68 \times 10^{19} \text{ cm}^{-3}$ heavy particles) at 19,000 °K at the tube center. The average heavy particle density is therefore $1.8 \times 10^{19} \text{ cm}^{-3}$ and compares to $1.6 \times 10^{19} \text{ cm}^{-3}$ of heavy particles for the Rankine-Hugoniot case assuming a temperature of 19,000 °K, the same initial conditions as the experimental gas, and no boundary region. Thus the 2.3 factor of disagreement between Rankine-Hugoniot theory and the spectroscopically measured particle density may be reduced to ~ 10 percent by the assumption of a Rankine-Hugoniot temperature equal to the spectroscopically observed temperature and a cool boundary region in the experimental gas diffusing into the hot plasma with equal pressures in the hot and cold gases²².

CHAPTER III

APPARATUS AND EXPERIMENTAL PROCEDURE

A. Introduction

In order to measure the shape of the (optically thick) N II and C II ion resonance lines and by fitting to calculated profiles, determine the Stark broadening effect, the electromagnetic T-type shock tube described by Elton^{20,21} which provides reproducible shock heated plasmas in the 20,000 °K ($kT = 1.7$ eV) range was employed as the radiation source. For both of these ions, the lines of interest lie in the vacuum ultraviolet (VUV) region of the spectrum, so that a vacuum spectrograph, namely a two meter normal incidence type, was utilized. The spectroscopic data for independent determination of the electron temperature and density was obtained in the optical region of the spectrum with two monochromators, one of which monitored the continuum radiation (N_e), while the other scanned the helium He I 4713 Å and the hydrogen H β 4861 Å spectral lines (N_e, T) and the He I 3889 Å line (N_e). The visible and VUV scans were performed simultaneously on a shot-to-shot basis. Spectral emission was detected by photomultipliers and recorded with oscilloscopes and cameras. Sodium salicylate was used as a VUV scintillator.

Regulation of plasma reproducibility from shot-to-shot was effected by a control of the total travel time of the shock wave. The data was measured 4 μ sec after the arrival of the shock front. Initial gas mixture ratios were maintained to 1.5% of partial pressure through fine metering valves and a capacitance manometer. The gas mixtures used were 40 torr helium with 400 mtorr H₂ and 100 mtorr N₂, and 40 torr helium with 200 mtorr CH₄.

B. Apparatus

Shock tube. The electromagnetic shock tube, optical set-up, detection and recording used is essentially as developed and described by Elton^{20,21} with some minor modifications. The shock tube employed is a 16 cm by 70 cm T-configuration, 2.5 cm I.D. with a 70 cm expansion tube, a 3 mm thick wall, and a 2.5 cm electrode spacing. It was found to achieve its best reproducibility at a helium pressure of ~40 torr and a capacitor (108 μ F) charging voltage of 8.7 kV. To perform properly at higher or lower pressures, higher and lower voltages must be used respectively. The 108 μ F capacitor bank is discharged into the tube with a quarter period of 10 μ sec. For the present experiment, 40 Torr of helium was used at a voltage of 8.7 kV $\begin{matrix} +200V \\ -100V \end{matrix}$. The voltage control was required to regulate the total shock travel times.

The shock wave is driven from the arc region through the dense ambient gas in the expansion tube. Separation of the shock wave from the arc plasma jet is clearly achieved at the high pressure and long expansion length in this device. This means that impurities associated with the plasma arc, namely electrode and tube wall material, are not present in the shock at the instant of observation downstream. In addition, the separated shock wave collides, after reflection at the observation end of the tube, with the arc plasma, slowing it down or even stopping it short of the observation region, with the result that about 2 inches at the observation end becomes clouded at a greatly reduced rate. What clouding formed (about a 15% drop in visible transmission over 250 discharges) was measured and corrected for in the data reduction. When the observation end became too cloudy from deposits, the reflector was removed and the observation end swabbed with hydrofluoric acid followed by water, and then with a dry swab. The reflector assembly was then reinstalled and the shock tube evacuated.

The driver section is constructed of aluminum oxide as shown in Fig. 2. The electrodes are of "Mallory Metal", a compressed sintered tungsten and copper alloy and are press-fitted to nickel electrode bodies which were drilled to provide for evacuation. This choice of materials permitted many firings. The aluminum oxide withstood an excess of three

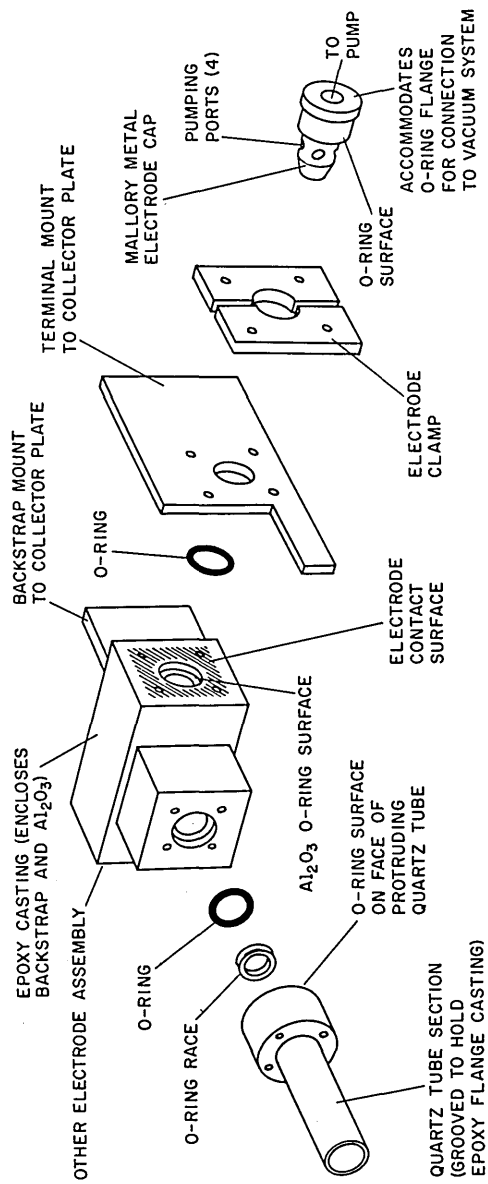


Fig. 2 - T-section assembly

thousand firings before breaking* It is also easy to clean by chipping out the deposit with a steel tool such as a screwdriver. The electrode surfaces become noticeably eroded asymmetrically on the expansion port side after about a thousand discharges, after which the electrodes were rotated to present a new surface to the arc path. In contrast, the surfaces of nickel electrodes became very irregular after a hundred shots, though it was not established that the condition of the electrode surface affected plasma reproducibility.

Single O-ring vacuum seals were seated on the (polished) aluminum oxide end surface and on the nickel electrode body shoulder (Fig. 2). The small clearance between the electrode body and the aluminum oxide inside surface cooled the plasma sufficiently so that erosion of the O-ring was negligible. The vacuum seal was made initially by atmospheric compression and then further compressed by the electrode clamps. Best results in terms of plasma reproducibility were obtained when the electrode tips were separated a tube diameter, i.e., 2.5 cm.

The electrode current collector plate to which the T-section is attached is mounted on a lath bed providing two degrees of freedom of positioning in the horizontal plane. Some degree of vertical

*Quartz and tempered Pyrex were also tried as arc section materials; the quartz broke after 20 firings and the Pyrex broke after 50 firings.

pitch is available at the T-section to-collector plate mounts. Displacement in other degrees of freedom required shimming of the lathe bed stand.

The number of firings between T-section overhauls was ultimately limited by the pumping port design. As firings progressed, hard deposits would diminish the clearance between the tube inner surface and the radially directed pumping ports in the electrode body, eventually sealing the ports. Especially heavy carbon deposits occurred on the walls of the driver section behind the electrodes and at the extremities of the arms. The hard deposits are readily chipped away from the Al_2O_3 for cleaning.

Care in disassembling the electrodes was necessary to avoid spalling of the Al_2O_3 O-ring surfaces when extracting the electrodes.

A 20 cm section of the 70 cm quartz expansion tube was bolted to the epoxy body of the aluminum oxide driver section through an epoxy flange cast to the quartz tube (Figs. 2 and 3). (Double grooves were ground on the quartz tube before casting to bind with the epoxy). The O-ring seal was supported on its I.D. by a stainless steel race. The remaining 54 cm of quartz tube was attached by a short section of rubber tubing. Any additional impurities provided by the rubber surface exposed to the plasma near the arc region would contribute negligibly to the already impurity-laden arc plasma, since the shock separation occurs further down

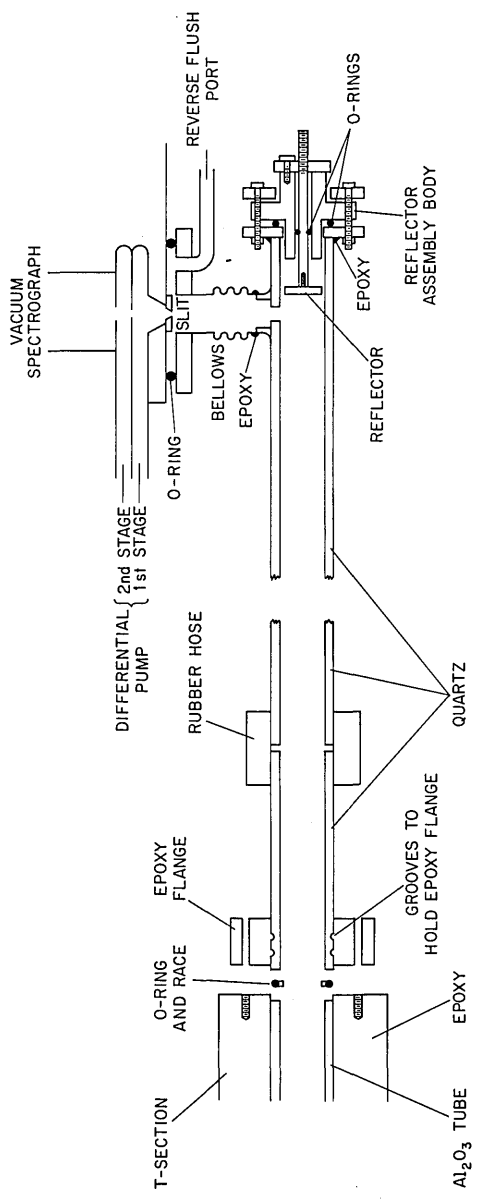


Fig. 3 - Mounting of expansion tube

the expansion tube. This flexible connection proved valuable in assembling, aligning and dismantling the shock tube. Since one end of the tube was connected by a side-on bellows to the vacuum spectrograph, the lateral displacement of 1/8 inch when evacuating the system might unduly strain the quartz tube in a rigid system.

A brass flange provided with an O-ring surface (Fig. 3) was vacuum sealed with epoxy to the observation end of the expansion tube (unannealed quartz tube end face was found to spall under O-ring compression). A second brass flange bolted to this served as a clamp for the reflector assembly and the O-ring seal. The reflector is mounted on a rod that accepts an O-ring on its circumference. This O-ring serves both as a vacuum seal and as a bearing when the reflector shaft is inserted through a polished hole in the reflector assembly body, and permits an axial adjustment of the reflector position from outside the vacuum region by a threaded nut attached to the end of the shaft. After positioning the reflector, this nut is bolted to the reflector assembly body in order that the reflector is not displaced by the impact of the shock wave.

A 5 mm x 5 mm square window was cut in the tube wall 2.5 cm from the reflector end of the 54 cm tube and a side arm of quartz was attached radially (quartz to quartz seal) for transverse (to the shock motion) VUV observation. A vacuum epoxy seal to the side arm was tried here and evidently suffered from stresses about the window corners, since the tube shattered in this region after a few discharges with

a quartz expansion tube and after about fifty shots with annealed Pyrex expansion tube (the annealed Pyrex showed no strains on a Polariscope about the window prior to application of the epoxy).

The side arm is vacuum epoxied to the bellows on the flange covering the slit face assembly of the VUV spectrograph. Disassembly is effected simply by applying a torch to the epoxy which soon softens. This flange also receives the reverse gas flush line for the spectrograph entrance slit (see Fig. 3). The vacuum epoxy^{*} used required 24 hours to cure to full strength, so that this method of assembly was only practical for joints that required infrequent assembly. Hastening the curing by heat resulted in poor vacuum seals, probably caused by expansion and contraction of the metal component whose thermal coefficient of expansion is ~ 25 times that of quartz.

Gas Mixing and Control Systems. Filling gas mixtures of 40 torr He, 400 mtorr H_2 and 100 mtorr N_2 for the N II experiment, and 40 torr He and 200 mtorr CH_4 for the C II experiment were found to provide a hydrodynamic shock with desirable plasma and spectral properties (see Chapters I and II). To keep the partial pressure of the test gas, N_2 accurate to 5 percent, the leak rate of the closed-off experiment volume with a base pressure of 5 mtorr should be no greater than 5 mtorr in ten minutes, the approximate fill-to-discharge sequence time. For the

* Torr-seal manufactured by Varian Associates, Vacuum Division, Palo Alto, California

discharge sequence required, it is necessary to be able to repeatedly fill the mixing volume to the desired constituent gas partial pressures without intercontamination of the gas reservoirs, to maintain reservoirs with leakage specifications comparable to the vacuum system, to have a pressure monitoring device with a broad range (about 10^4) and with a time constant short enough to follow pressure changes of the system as gas escapes through the spectrograph slit. In addition, it is very desirable that the pressure gauge be insensitive to gas composition.

The gas mixing system chosen (see Fig.4) fills a common mixing volume from each of three gas reservoirs through fine leak valves, and uses one pressure sensing station at the mixing tank. A capacitance manometer* satisfying the pressure range requirements (30 mtorr - 100 torr full scale), time constant (100 μ A meter), and independence of gas composition to 5% accuracy⁵⁶ was employed. Intercontamination of reservoirs is given by

$$\frac{\Delta P}{P_1} \propto \left(\frac{P_2}{P_1}\right)^2 \frac{V_2}{V_1} \approx 10^{-7} \quad (42)$$

*Type 77 H-100 Baratron manufactured by MKS Instruments, Inc., Burlington, Massachusetts.

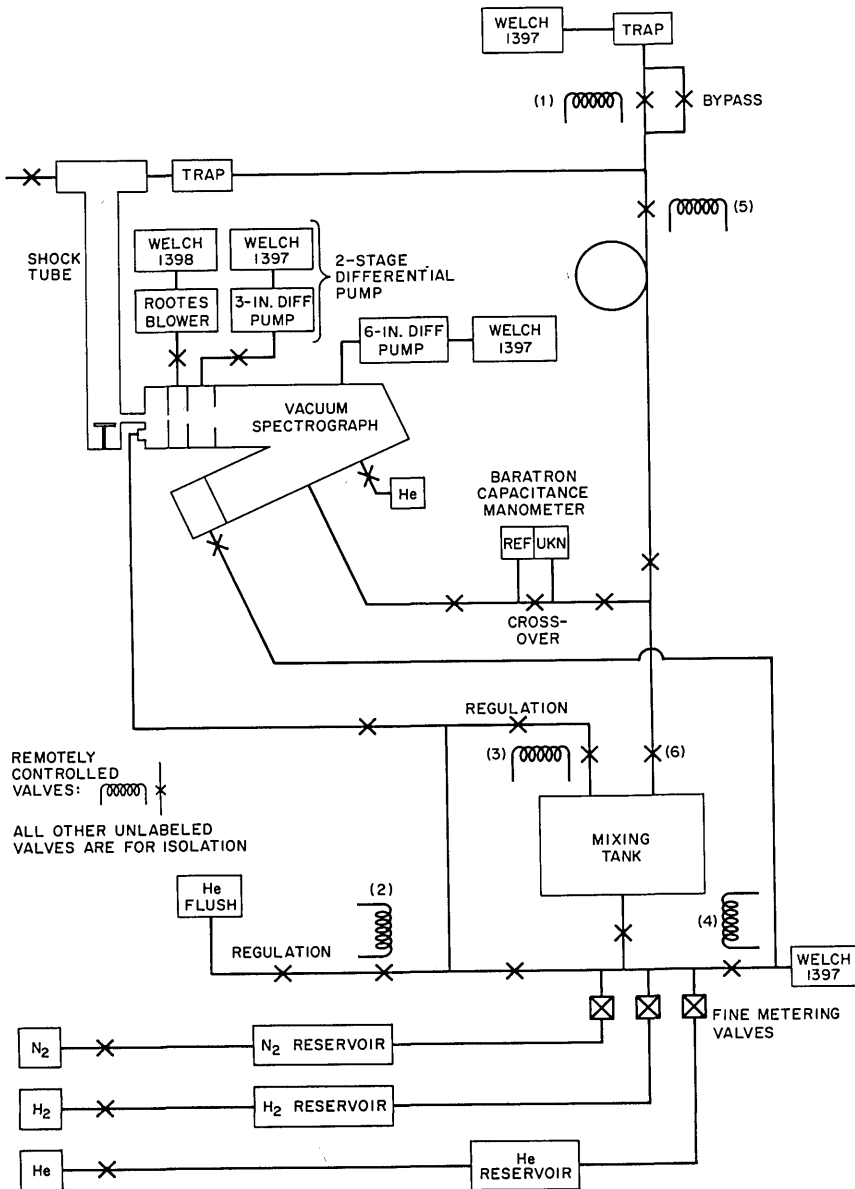


Fig. 4 - Vacuum, gas mixing, and reverse flush system

where the subscripts 1 and 2 refer respectively to the high pressure side (volumes equal 0.25 ℓ for H₂ and N₂, 3 ℓ for He, pressure equals 1.7 atm for all three) and to the mixing tank side (2.5 ℓ volume for all three) where the helium is introduced last.

Requirements on the leak valves are rather severe. They must be capable of speeds of $\sim 10^{-5}$ ℓ/sec to control pressures in the mixing tank to a few percent at 0.1 torr against a supply pressure of 1.7 atm; they must shut off with a maximum speed of $\lesssim 10^{-8}$ ℓ/sec) and they must provide high speed (0.15 ℓ/sec) for purging the fill lines. In particular, the leak valve itself must be used to isolate the volumes. Otherwise, with an auxiliary shut-off valve, the volume between leak valve and the shut-off valve rises to pressures of the order of an atmosphere, which would require each gas line to be pumped while another is being used. Valves meeting these requirements were found to be available.* Reliable magnetically actuated air-operated and manual off-on valves[†] providing excellent isolation were employed. A number of other manufacturers' valves were found to either leak across the seat or to leak from atmosphere at the bellows. Copper refrigeration line 3/8" O.D. soft-soldered at connections

*Series 203 manufactured by Granville-Phillips Co., Boulder, Colorado.

†Types FL, FR 385, FPL 625 (remote) and FL 625 manufactured by Vacuum Electronics Inc., New York.

was used throughout the vacuum system.

The isolated pressure rise rate was found to be 0.3 mtorr/min (10^{-8} μ /sec) for the mix-system, 0.3 mtorr/min (10^{-9} μ /sec) for the shock tube.

It was found necessary to maintain the integrity of these vacuum specifications in the construction of the feed lines and reservoirs and to provide an isolation valve between the gas bottle regulator and the system to avoid contamination of the majority gas (He), principally, by atmospheric nitrogen due to diffusion through connections or the regulator itself. A previous line of vacuum hose either leaked or outgassed with an equivalent throughput of 4×10^{-4} torr μ /sec (0.1 torr estimated partial pressure in the gas mixture), quite sufficient to provide signals whose intensity was directly related to the time the supply gas had remained in the supply line prior to firing. After replacement of this line by a leak-checked copper one, minimal contamination was encountered as indicated by the independence of the data with respect to the age of supply gases and by low intensity (about 8%) of the continuum signal of 40 torr He relative to the signal obtained in the gas mixture 40 torr He, 0.4 torr H₂ and 0.1 torr N₂. The continuum signal from pure helium reached maximum about 7 - 8 μ sec after shock arrival in contrast to 3 μ sec for the signal from the gas mixture. The addition of 5.0 mtorr H₂

or N_2 was observed to substantially shorten this rise time.^{22,23} The observation of the radiation of shocked 100% He therefore served as a sensitive indication of contamination of the helium supply, accordingly estimated as less than .025% or less than 0.01 torr partial pressure of the gas mixture. "Warmup" shots were unnecessary at the start of a day's scan. After initially purging and filling the gas supply lines, the first shots fell within the scatter of the previous day's last shots, providing, of course, that the arrival time criterion was satisfied, as was usually the case.

Each soft soldered joint outgassed considerably at first; however 24 hours of pumping was sufficient to reach the required leak rate. Careful application of heat by a propane torch considerably hastened outgassing, but usually was not worth the risk of unsoldering the joints, since temperatures for rapid outgassing approached solder melting temperatures. Vacuum epoxy (see footnote, p.36) was quite adequate at dissimilar material connections involving glass, stainless steel, brass, and soft copper (must be tinned with solder), although such joints do not offer much resistance to mechanical stress and must be supported where stresses are expected. Thermal setting vacuum epoxy* was also used, but was found to be more brittle mechanically and difficult to remove.

*Manufactured by Plastic Associates, Laguna Beach, California.

A reverse flushing system was required to remove granular material (Al_2O_3) from the 0.025 mm wide spectrograph entrance slit. Consequently both the electrode (1) and the helium flush valves (2) as indicated in Fig. 4 were opened shortly after discharging the capacitor bank. The regulating valve for the flushing line was set for a pressure of 80 torr with valves (1) and (2) open.

The mixing system is shown in Fig. 4. The Baratron vacuum gauge utilized the vacuum spectrograph vacuum as the reference vacuum ($\sim 5 \times 10^{-6}$ torr). With valves (3) and (5) closed and (6) open it monitors the mixing tank pressure. With (4) and (5) closed and (3) and (6) open, it monitors the tube pressure through the slit chamber. With (6) closed and (5) open it measures tube pressure through the pumped electrode. With (1) and (2) open, the difference in pressures between the slit face and the pumped electrode indicates any plugging of the pumped electrode. With (1), (2), (4) and (5) closed, the rate of pressure drop indicates the degree of plugging of the spectrograph slit.

The control sequence (in relation to the operation of the valves) (see Fig. 4) is as follows: assuming the capacitors have just been discharged, valves (1) and (2) are open for shock tube flushing, (3) is closed, (6) is open, (4) is open, and (5) is closed (mixing tank being evacuated). Then valve (2) is closed (tube being evacuated). Valve (4) is then closed and the gases are introduced into the mixing tank in the order N_2 (175 mtorr), H_2 (700 mtorr) and He (70 torr). The Baratron gauge is then set to null at 42.5 torr. Valve (1)

is closed and (1), (2) and (4) are set to open automatically shortly after the tube is fired (any delay being determined by relay closing time plus the valves' reaction times following the main bank trigger pulse). Next, valve (3) is opened and the gas mixture fills the shock tube and escapes through the spectrographic slit. When the Baratron indicates a null, valve (3) is closed, the main bank is isolated electrically from the power supply, and the trigger switch is closed. From the time valve (3) is closed until the trigger actually fires, the tube drops in pressure about 2 torr, and with care the pressure at firing was within ± 200 mtorr of 40.5 torr, i.e., $\pm 0.5\%$. The trigger pulse actuates a relay which in turn opens valves (1), (2) and (4), thereby flushing the tube and evacuating the mixing tank.

Opening valve (3) actuates a preset timer and alarm. If the alarm sounds before the Baratron nulls, it is an indication to the operator that the slit has clogged and that it is necessary to clear the slit by filling the spectrograph with helium and pumping through the shock tube.

Capacitor bank and discharge circuit. These are described in more detail by Elton.²⁰ Briefly, a low inductance 0.1 μ fd, 40 kV capacitor* is charged by a 25 kV power supply

*Type NRG.341 manufactured by Tobe Deustchmann Corp., Norwood, Mass.

until an air-gap switch over-voltages (this takes a substantial fraction of a second) discharging the capacitor energy into each of seven triggertron⁵⁷ switches and providing a trigger pulse for the oscilloscopes. The main capacitor bank consists of fourteen 7.7 uf 20 kV Bosch capacitors (108 μ fd total) connected in parallel and charged to about 8.7 kV. They are discharged in parallel (two capacitors per switch) through 28 coaxial cables into a collector plate to which the T-tube electrodes are connected with a low inductance near return conductor to provide additional magnetic propulsion.⁵⁸ The peak current is about 500 kA with a ringing period of about 18 μ sec, damped to \sim 10 percent in two cycles. The inductance is 34 nH and the total resistance is 0.01 Ω .

The sequence for charging and discharging the capacitor bank is as follows: The mechanical shorting devices are removed and the power supply connected (by relays) to the main bank through charging resistors. The capacitors charge in about 40 seconds at a 25 mA rate. At the desired voltage (monitored by a precision electrostatic voltmeter^{*}), the charging current is set to zero. The valves are then set and the gas mixture is let into the tube as described above. While the final firing pressure is approached (\sim 7-15 seconds) slight adjustments to the voltage can be

*Type 51B, Rawson Instr. Co., Cambridge, Mass.

made. The final voltage is noted, valve (3) (Fig. 4) is closed, the high voltage isolation switch is opened, and the discharge switch is closed. The trigger capacitor over-voltages the air-gap switch thereby triggering the main discharge. A relay is then closed to remove any residual charge through resistors, the mechanical shorting bars lowered, and the tube is allowed to flush for about 30 seconds.

This system has performed quite reliably, any irreproducibility being caused by a deterioration of the main bank switch electrodes or trigger pins or by a leak in the vacuum system. A cleaning of the main bank switches is indicated by difficulty in maintaining a constant voltage during the interim period just prior to discharge. A few initial pre-discharges sometimes occurred when the ambient relative humidity approached 70 percent.

Optical system. The optical system consisted of two 500 mm focal length monochromators* and a 2 m normal incidence vacuum spectrograph†. The visible scanning monochromator was blazed for 3000 Å and the continuum monochromator for 5000Å. Both monochromators have a 1200 lines per mm plane grating and a reciprocal dispersion of 16.5 Å/mm. The

*Bausch and Lomb Inc., Rochester, N.Y.

†Model 240 McPherson Inst. Corp., Acton, Mass.

scanning monochromator was set to a full half width of 1.3 \AA and the continuum monochromator to 22.5 \AA as determined by photoelectrically scanning the 2536 \AA mercury line of a pen-ray lamp*. The monochromators were aligned by reverse illumination by lamps† from the position of their photomultipliers, and the image of their entrance slits focused near the center of the shock tube. The entrance slits were adjusted to give superimposed $1 \times 5 \text{ mm}$ projections at the shock tube axis 3.4 mm from the reflector. The mirrors were so adjusted that reflected light from the slit of one monochromator did not enter the optics of the other. The visible optics alignment was made with the shock tube under vacuum to allow for the compression of the connecting bellows. The grating of the 2m normal incidence vacuum spectrograph (1200 lines/mm , 3.75 \AA/mm reciprocal dispersion) was likewise reverse illuminated, the beam emerging from the entrance slit at 3.4 mm from the reflector. The instrumental width of the vacuum spectrograph was determined to be 0.14 \AA by a photoelectric scan of the 2536 \AA mercury line of the pen-ray lamp.

Neutral density filters used to adjust the luminosity to match the dynamic range of the system were Bausch and Lomb reflectance filters of density 1.2 for the scanning monochromator

*Mod. SCT-1, Ultraviolet Products, Inc. San Gabriel, Calif.

†American Optical Co., Instrument Div., Buffalo, N.Y.

and 0.6 for the continuum monochromator and were checked for absolute density value and for wavelength dependence by a spectrophotometer*. The densities of these filters were found to be wavelength independent in the 5500 Å - 4500 Å and 4000 Å - 3500 Å ranges, quite in contrast to Kodak Wratten filters, particularly in the latter range where the Wratten filters' density increased rapidly with decreasing wavelength.

Electronic systems. The light signals were detected by photomultipliers whose outputs were recorded by oscilloscopes. The photomultipliers were EMI† 6256 for the visible continuum radiation monitor, EMI† 6255 for the visible scanning monochromator, and EMI† 6255 for the VUV spectrograph. Their dark currents were 0.5 nA, 1.0 nA, and 20 nA respectively. The high voltage supplies** were operated at -1400 V, -1700 V and -1300 V, respectively. All signal cables (RG 9 B/U) were terminated in 50Ω and the signals were smoothed with passive integrator circuits. The time constant was 0.1 μsec for the visible and 0.2 μsec for the VUV signals.

*Carey Instruments, Applied Physics Corp., Monrovia, Calif.

†Manufactured by EMI, Ltd. Hayes, Middlesex, England. Distributed by EMI/US, Westbury, L.I., New York.

**Mod. 405 and 412A, John Fluke Mfg. Co., Seattle, Washington.

Each photomultiplier was placed in the visible monochromator and checked for linearity at 6210 Å with a succession of Kodak* Wratten neutral density filters of varying density placed in the optical path (at this wavelength these filters were close to their rated density). The shock tube was used as a source and monitored simultaneously by an auxiliary monochromator at the same wavelength. The optical detection system was linear (slope=1.025) with current from 1 mA to 14 mA and indicated a saturation at 20 mA. Throughout the experiment the photomultipliers were therefore operated at less than 10 mA peak signal current.

Two Tektronix type 555† dual-beam oscilloscopes were used to display the photomultiplier signals and the dI/dt signal obtained from an inductive loop placed near the shock-tube electrodes. The dI/dt trace was triggered by a signal from the trigger capacitor discharge, as was the 555 delay circuitry. After a 50 μ sec delay, the VUV sweep (555) started and triggered the sweep for the continuum and visible scan signals. The + gate of the dI/dt sweep circuit triggered a Tektronix type 545 oscilloscope (set for a one second full sweep time) which provided an actuating signal

*Eastman Kodak Co., Rochester, N.Y.

†Tektronix, Inc., Beaverton, Ore.

of 25 V (by its + gate) to the latching control relay for valves (1), (2) and (4) in Fig. 4. The signal traces were photographed on Polaroid* type 47 film by two Tektronix C-12 cameras.

C. Experimental Procedure

The VUV N II and C II multiplets were first obtained on photographic film in order to determine the concentration of test gas for which the plasma was not so optically thick that the individual multiplet members could not be resolved. One hundred mtorr was chosen as the partial pressure for the N₂ gas with 400 mtorr H₂ added and 200 mtorr as the partial pressure for CH₄. About 20 shots in 40 torr He were required to expose the Kodak SWR film satisfactorily and about 3 shots for the Kodak 101-01-05 film.

A preliminary simultaneous scan of both VUV and visible lines (2 shots per point) was performed to determine signal levels and the precise location of the VUV lines on the spectrograph wavelength scale.

Subsequently a more detailed scan was performed. The gas mixture selected was 40 torr He, 400 mtorr H₂ and 100 mtorr N₂. A number of shots were taken at each point of the spectrum and the capacitor voltage adjusted slightly as necessary such that the shock arrival times remained within ± 0.4 μ sec of 54 μ sec for at least five

*Polaroid Corp., Cambridge, Mass.

shots. While the N II multiplet was being scanned in the VUV the visible shot-to-shot scan at 20 Å intervals was started at 4551 Å and continued to the wing of the He I 4713 Å line. Ten Angstrom intervals were taken through each half halfwidth and 5 Å intervals across the peak. The H β 4861 Å line was scanned at 10 Å intervals up to 4891 Å (Fig. 5). The continuum signal at 5423 Å was also taken as a data point by this monochromator. A repeat rough scan consisting of three acceptable shots per wavelength plus the maxima and halfwidth points of the lines and the continuum at 5423 Å was then made. The instrument width was 7 Å.

A tungsten lamp was then used as a source for a relative intensity calibration with respect to wavelength of the visible monochromator-photomultiplier system. The brightness temperature of the lamp versus the regulated direct current was obtained from a National Bureau of Standards calibration. The brightness temperature was converted to equivalent blackbody temperature from which a relative intensity was obtained.⁵⁹ The correction of the He I 4713 Å signal relative to the H β 4861 Å signal was 20 percent which lowered the uncorrected temperature by 1.7 percent. The photomultiplier direct current signal was about 0.02 percent that of the dynode voltage divider current.

The C II scan (Fig. 7) was performed with an instrument width of 0.14 Å in the VUV and 1.3 Å in the visible. The gas mixture was 40 torr He and 200 mtorr CH₄. The VUV scan was toward longer wavelengths and the scan was ended

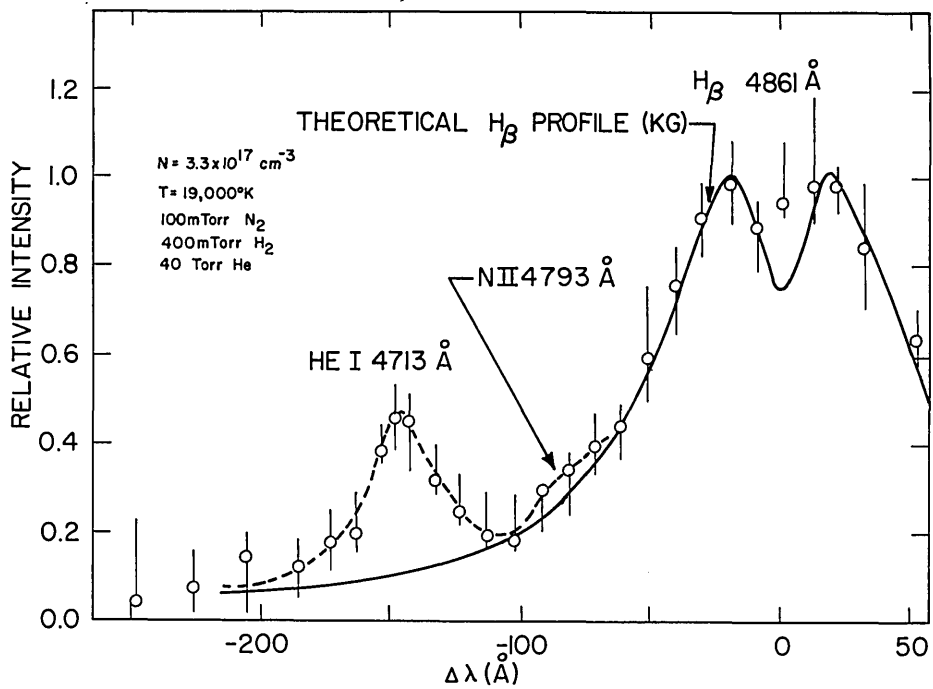


Fig. 5 - Profiles of He I 4713 Å and H_β 4861 Å

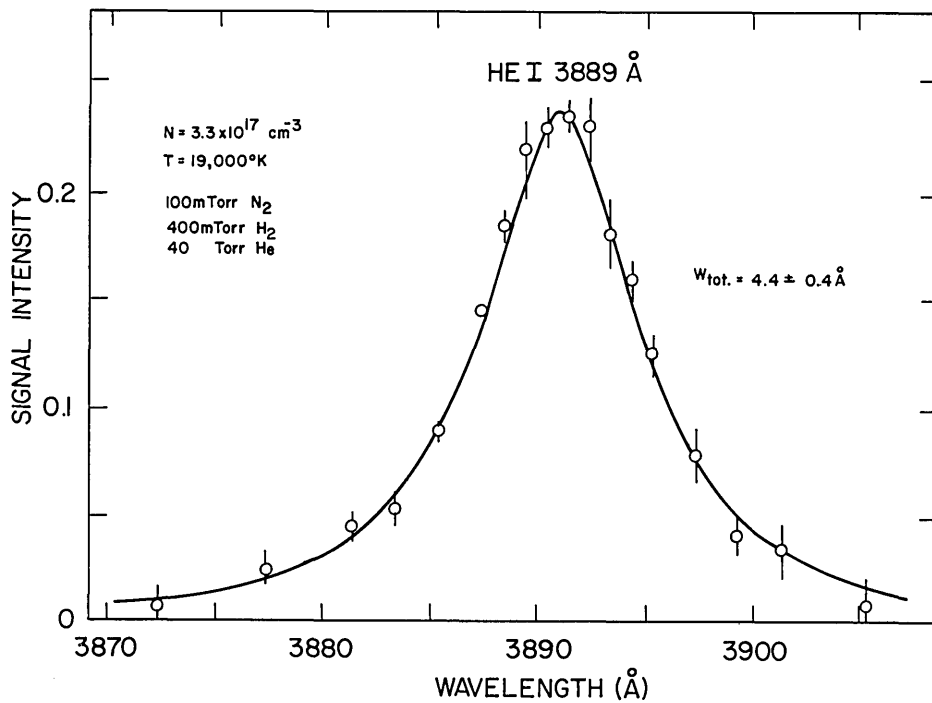


Fig. 6 - Profile of He I 3889 Å

by rescanning the short wavelength wing and peak. At the short wavelength peak the concentration of CH_4 was varied and compensating amounts of H_2 added (to maintain the same hydrogen concentration as at the nominal carbon concentrations). This procedure defined the blackbody limit. The He I 3889 was scanned on the short wavelength wing and at 2 \AA intervals through the short wavelength half intensity point and peak.

The N II multiplet (Fig. 8) was scanned again from lower to higher wavelengths with an instrument width of 0.14 \AA in 0.075 \AA steps with three acceptable shots per point. The blackbody limit was confirmed as before. During the scan "pure" helium and hydrogen compensated nitrogenless shots were made on the wings and line centers to monitor the background nitrogen, which was deduced to be ~ 5 mtorr. This technique was useful in detecting vacuum leaks that occurred during the scan.

At the long wavelength peak of the profile, the helium-methane mixture used in the C II scan was substituted with enough nitrogen added to establish the blackbody limit in order to confirm that the temperatures of the two experiments were the same. The He I 3889 \AA line (Fig. 6) was scanned twice at 1 \AA intervals over the peak and half-intensity points to confirm that the electron density was the same in the two experiments. The He I 4471 \AA wing, He I 4713 \AA wings and peak, and H β 4861 \AA wings and peaks and the VUV blackbody levels were observed to confirm that the temperatures of the two N II scans were the same. The visible monochromator instrumental halfwidth was 1.3 \AA .

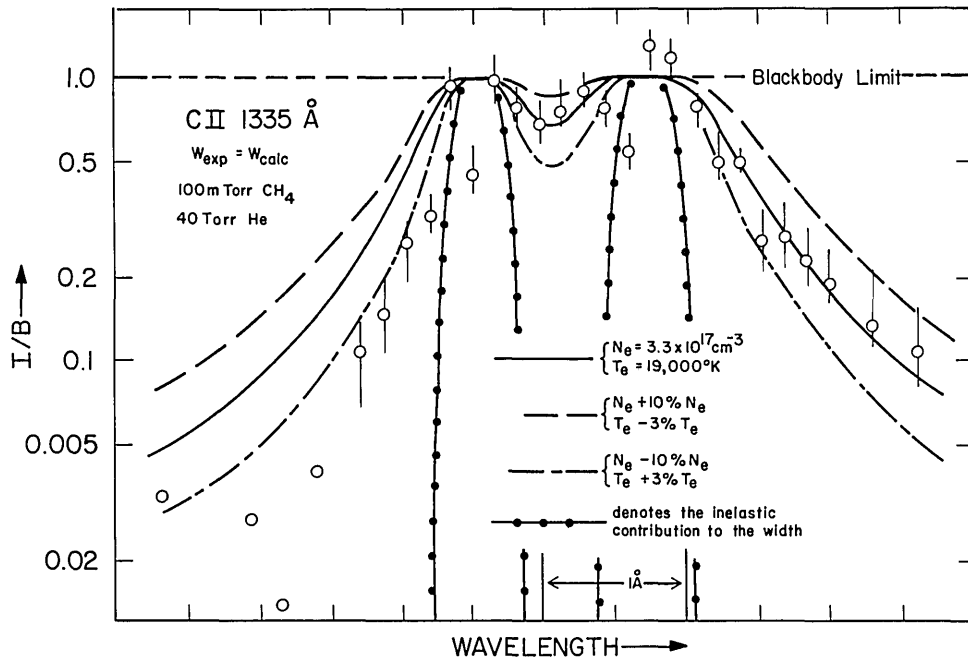


Fig. 7 - Profile of C II 1335 Å

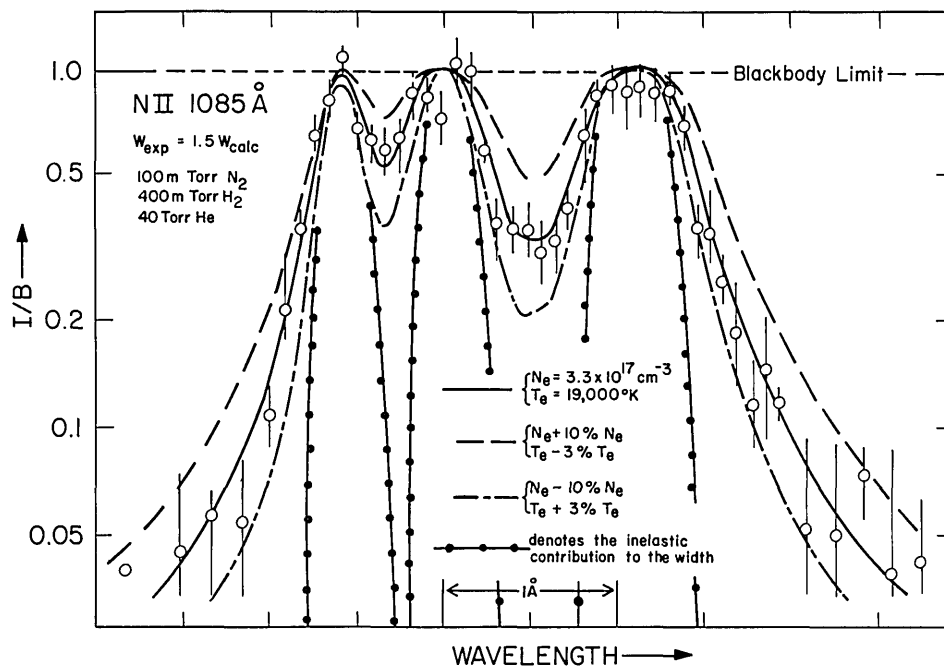


Fig. 8 - Profile of N II 1085 Å

Finally the short wavelength wing and peak were scanned in order to detect any systematic errors in the profile scan of N II.

The continuum at 5423 Å (chosen for the lack of impurity lines) was scanned over a ± 14 Å range with a 2 Å instrument width. The scan indicated no observable line emission for the times of interest. Time integrated spatially resolved photographs on Kodak 103-F film using a Zeiss prism spectrograph had also indicated no line emission near this wavelength at the observation region in front of the reflector. The continuum monitor served two purposes. It provided a relative measure of the electron density since in the data analysis the scan signals are read at constant electron density. Also, since the optical transmission of the tube was decreasing with each shot, the maximum continuum signal provided data on this trend useful for a correction to the visible line-scan signal amplitude.

The scans, at a rate of about 1 shot per 15 minutes, required about 60 hours over six days. The oscilloscopes were calibrated before and after a day's run. The VUV scanning mechanism was energized between each scan point for 24 seconds for the first N II scan, 18 seconds for the second N II scan, and 36 seconds for the C II scan, at a rate of 0.25 Å/min. Some coasting of the scanning mechanism following deenergizing was measured. Therefore a continuous scan over 15 Å was made and compared to the same scan (150 steps) made in 24 second increments, to provide a coasting correction

of $\sim 7\%$ to the wavelength scale for the rate used.

After each ten shots the helium line was purged with fresh helium as a precaution against contamination (see "Gas Mixing and Control Systems") and the depleted reservoir replenished. After each three to ten shots the vacuum spectrograph was filled with helium while the shock tube was pumped down to flush the entrance slit. Before and after such reverse flushings of the spectroscopic slit, the time was recorded during the first N II scan for pumping the tube down through the slit by the differential pumping system from 42.50 torr (originally filled to 70 Torr helium) to 15.64 torr, i.e., 42.50/e. The improvement in slit speed with each flushing amounted to about 10% but the trend indicated a gradual irreversible plugging of the slit. During subsequent scans the pumpdown time to firing pressure was monitored and the first stage differential pump foreline pressure noted during the reverse flushing of the shock tube after each shot. The pumpdown time, foreline pressure and VUV signal intensity correlated to indicate progressive slit plugging with each shot for a series of shots between slit flushings, particularly near the end of a scan. Manually cleaning the exterior side (shock tube side) of the slit did not improve its speed. The visible optical alignment after the run was rechecked. No misalignment was found.

CHAPTER IV

DATA REDUCTION AND ANALYSIS

The oscilloscope signals for the photomultipliers and the dI/dt pickup loop were recorded on Polaroid film. The experiment was monitored by the signal amplitude at a time $4 \mu\text{sec}$ behind the shock front.

A. The Continuum Signal

All data for shots for which the time from trigger capacitor firing to start of signal at the observation position (reflected shock) exceeded $54.2 \mu\text{sec}$ or was less than $53.8 \mu\text{sec}$ were discarded. These amounted to about 6 percent of the shots.

Since the continuum signal is proportional to the square of the electron density,¹ a constant amplitude was chosen for data analysis, so that the points of the spectral profiles would all correspond to the same electron density. This constant continuum signal amplitude was chosen to be less than the peaks of 90 percent of the signals and determined the time following the shock arrival at which the visible and VUV signals would be read on a particular shot. This time varied about the $4 \mu\text{sec}$ point after shock arrival by $\pm 0.4 \mu\text{sec}$.

B. The Visible Scan Data

The visible signals corresponding in time to a constant electron density were plotted versus wavelength on linear graph paper with corrections for the calibrated neutral density filter and oscilloscope attenuation factors included.

The electron density was calculated from the half-width of He I 3889 Å (Fig. 6) from the formula^{1,35,44}

$$W_{tot} \approx [1 + 1.75 \alpha (1 - 0.75 r)] w N_e \times 10^{-18} \text{ Å} \quad (43)$$

and the value of w ⁴⁴ and α ³⁵. Here w is the width from electron impacts, α is the quasistatic ion broadening parameter, and r , the Debye shielding parameter, is the ratio of the mean ion separation to the Debye radius. The total line halfwidth, W_{tot} , is determined from the measured width of the profile and the halfwidth (1.3 Å) at half maximum of the scanning monochromator (Gaussian) instrument function^{38,61}.

Analysis of the visible data proceeded as follows: The prominent features of the scan were the He I 4471 Å wing, He I 4713 Å, and H β 4861 Å. It was desired to obtain the electron temperature from the ratio of total intensities of He I 4713 Å to H β 4861 Å. Calculations showed that the H β peak intensity plus the underlying continuum intensity

should be 11 percent optically thick, i.e., for H β to be fully represented for temperature measurements, the peak signal should be multiplied by 1.1 to provide equivalent optically thin data. After corrections for the instrument relative wavelength response (Chap. III) and the plasma optical depth were made, continuum and He I 4471 Å contributions were estimated by

$$I(\lambda_1) = \frac{A}{(\lambda_1 - \lambda_0)^2} + I_{cont} \tag{44}$$

$$I(\lambda_2) = \frac{A}{(\lambda_2 - \lambda_0)^2} + I_{cont}$$

where $I(\lambda_1)$ and $I(\lambda_2)$ are the signals at two wavelengths on the He I 4471 Å wing, A is a constant, λ_0 the line center (4471 Å) and I_{cont} the continuum intensity. Eqs. (44) were solved simultaneously for A and I_{cont} , errors in the wing representation having a second order effect. The resulting continuum was checked against the measured continuum at 5040 Å and 5423 Å which had been corrected for instrument wavelength response.

The corrected signal for He I 4713 Å and H β 4861 Å above continuum and corrected for He I 4471 Å is represented in Fig. 5. A plot of H β from the tables for the H β shape function⁶² using the electron density determined from He I 3889 Å fitted the plotted data.

The total line intensity is given by

$$I = \int_{-\infty}^{\infty} I(\lambda) d\lambda = I \int_{-\infty}^{\infty} S(\alpha) d\alpha$$

since $\int_{-\infty}^{\infty} S(\alpha) d\alpha = 1$ From

$$I(\lambda) d\lambda = I S[\alpha(\lambda)] d\alpha$$

one obtains

$$I = \frac{I(\lambda)}{S[\alpha(\lambda)]} \frac{d\lambda}{d\alpha} = \frac{I_{\max}}{S_{\max}} \frac{d\lambda}{d\alpha} \quad (45)$$

where λ is chosen for convenience at the maximum of $I(\lambda)$ and $S[\alpha(\lambda)]$. The ratio, $\frac{d\lambda}{d\alpha}$, is given by the relation between α and $\lambda - \lambda_0$, $\alpha = \frac{|\lambda - \lambda_0|}{2.61eN_e^{2/3}}$ for H β and $\alpha = \frac{|\lambda - \lambda_0|}{w_{\text{tot}}}$ for He I 4713 Å where w_{tot} is given by Eq. (43) and Oertel⁴⁴. For He I 4713 Å S_{\max} is $1/\pi$ while S_{\max} for H β is obtained from Kepple and Griem⁶². I_{\max} is obtained from the H β and He I 4713 Å data. From the electron density calculated from the He I 3889 Å halfwidth, w_{tot} (4713) and $d\lambda/d\alpha$ were calculated and the ratio $I(4713)/I(\text{H}\beta)$ provided the electron temperature from computer tabulations based on Eq. (29), Chap. II.

C. The VUV Scan Data

The VUV data was measured from the Polaroid film at a time after shock arrival determined by the corrected constant continuum signal, and plotted on semilog graph paper, with the wavelength scale adjusted for scan-step overrun (see Experimental Procedure, Chap. III). The N II data were averaged at each wavelength point over 3 shots and the background signal subtracted. The graph was then compared to computer plots (also semilog) to ascertain the factor of agreement with the theory.

The computer plots represented an envelope of optically thick Lorentz profiles into which the instrument profile had been folded for six overlapping lines in a family of three curves, each curve corresponding to halfwidths which were 0.55, 1.0 and 1.8 times the experimental halfwidth to compare results using the estimated maximum experimental error in electron density and temperature (Fig. 7 and 8). The computer calculated the half halfwidth w_{calc} from Eq. (11), the effective absorption coefficient from Eq. (33), and the fractional blackbody intensity from Eq. (30). For N II there are six transitions involved, 1085.701, 1085.546, 1085.529, 1084.580, 1084.562, and 1083.990 Å⁶³ with different statistical weights and absorption oscillator strengths, so that

$$g_n f S(\lambda) = \sum_{i=1}^6 g_{n_i} f_i \frac{1}{\pi \left[1 + \left(\frac{\lambda - \lambda_{0_i}}{w_{\lambda}} \right)^2 \right]} \quad (46)$$

and $\kappa'(\lambda)$ becomes

$$\kappa'(\lambda) = \frac{\lambda^2 r_0 N^+}{w_\lambda Z^+} \sum_{i=1}^6 g_{n_i} f_i / \left[1 + \left(\frac{\lambda - \lambda_{0i}}{w_\lambda} \right)^2 \right] \quad (47)$$

The oscillator strengths given by Wiese, Smith and Glennon¹⁸ are scaled by the ratio 3.7/5.7, namely the ratio given by the experimental multiplet transition probability found by Lawrence and Savage¹⁹ (considered to be the more reliable) to that listed by Wiese et al.

The computer calculated (where $\tau = \kappa' d$ is the optical depth)

$$C + D \log \left[\int_{\lambda' = \lambda - 2\eta}^{\lambda' = \lambda} \{1 - \exp[-\tau(\lambda')]\} \left\{ 1 + \frac{1}{2\eta} (\lambda' - \lambda) \right\} d\lambda' \right. \\ \left. + \int_{\lambda' = \lambda}^{\lambda' = \lambda + 2\eta} \{1 - \exp[-\tau(\lambda')]\} \left\{ 1 - \frac{1}{2\eta} (\lambda' - \lambda) \right\} d\lambda' \right] \quad (48)$$

where η is the half halfwidth of the instrument and where C positioned the plot and D was chosen to give a 10 db displacement equal to one cycle of the graph paper of the data plot. Plots of I/B for widths $w_\lambda = 1.5 w_{\text{calc}}$ times the factors of experimental error were made and are compared with the data for N II in Fig. 8.

The C II analysis was similar to the N II analysis, there being three transitions at 1335.7077, 1335.6627, and 1334.5323,⁶³ and the data averaged over 5 shots per wavelength position which were taken at intervals of

0.15 Å rather than at 0.075 Å. The Lawrence and Savage correction gave oscillator strengths 2.56/6.0 times those of Wiese et al., and the plots of I/B were for widths $w_{\lambda} = 1.0 w_{\text{calc}}$ times the factors of experimental error and are compared with the data for C II in Fig. 7.

CHAPTER V

RESULTS AND DISCUSSION

A. Results and Error Estimates

Figures 7 and 8 present the experimental profiles of the C II (1335 Å) and N II (1085 Å) multiplets together with the theoretical profiles (solid curves) that best agree with the experimental points for $T_e = 19000$ °K and $N_e = 3.3 \times 10^{17}$ cm⁻³. The two (dashed) companion curves in each figure are the theoretical profiles corresponding to the experimental uncertainties (see below), i.e., $T_e + 3$ percent, $N_e - 10$ percent (lower curve) and $T_e - 3$ percent, $N_e + 10$ percent (upper curve), where the width is allowed to change with temperature and density according to the semiempirical approximation. Included here also are the profiles that would be expected if the broadening were only due to inelastic (dipole) collisions. For N II, the experimental width deduced from the effective absorption coefficient using a Lorentz line shape [Eq. (33)] together with the integrated equation of radiative transfer [Eq. (30)] is 0.0057 ± 0.0019 Å, that is, 1.5 times the width of 0.0038 Å calculated from the semiempirical approximation for the same electron temperature and density, as indicated in Fig. 1. The corresponding experimental width for C II is 0.0088 ± 0.0044 Å to which the theoretical width agrees to a factor-of-unity (Fig. 1) (the asymmetry of C II remains unexplained (see below)).

The inelastic contribution to the width, that is, the contribution of the portion of Eq. (10) for which $E \geq \Delta E$ in the integration over v , is seen to be $0.0036 w_{\text{calc}}$ (negligible) for $kT = 0.18 \Delta E$ here (Figs. 1, 7 and 8)

Figure 5 shows the profiles of the He I 4713 Å and H β 4861 Å lines obtained for two N II scans. The ratio I_{4713} / I_{4861} of the total intensities varies 13.5 times as fast as the temperature which it determines near 20,000 °K. Thus estimated experimental uncertainties of ± 30 percent in I_{4713} and ± 10 percent in I_{4861} result in a ± 3 percent uncertainty in the temperature.

The comparison of the blackbody limits at N II 1085 Å for both the C-H-He (+N) plasma and the N-H-He plasma agreed to within ± 20 percent, which also corresponds to a ± 3 percent remaining uncertainty in temperature for the C II data.

The uncertainty in the halfwidth determination of the He I 3889 Å line (Fig. 6) is estimated to be ± 10 percent. Thus a ± 10 percent uncertainty is estimated for the electron density.

Systematic errors in the visible diagnostics estimated from relative measurements of the shock tube wall transmission before and after a visible scan, relative calibration of the photomultiplier linearity (using the shock tube as a source), and a relative intensity

tungsten lamp calibration of the visual scan detection system (see Chap. III, Experimental Procedure) resulted in approximately a 2 percent correction (reduction) in the measured temperature.

Uncertainties in the VUV scan appeared to be due largely to a partial clogging of the slit (See Chap. III, Experimental Procedure). However, the average aperture of the slit was maintained essentially constant throughout the scan as indicated by a final rescanning of the first multiplet member from the wing to the blackbody limit. Scatter in the data was seen to fall within the estimated errors in the temperature and density (Figs. 7 and 8).

The asymmetry of the C II scan is greater than that due to ion broadening¹ (which contributes about 10 percent to the intensity at the half-intensity point and about 20 percent on the far wings), and is not evident on the N II profile. The centers of the C II multiplets also indicate strong self-absorption not as evident on the narrower N II peaks. A shift toward shorter wavelength is indicated for the self absorption in the C II multiplet, which is not in disagreement with a calculated Doppler shift due to a cold ion shock wave travelling toward the spectrograph slit from the shock tube through the connecting tube at about 1 cm/ μ sec.

B. Conclusions

The experimental profiles presented in this report represent the first reported observations of spectral line broadening due entirely to "elastic" electron collisions in an LTE plasma. Here "elastic" refers to collisions other than inelastic collisions through dipole interaction.

The semiempirical approximation (for a Gaunt factor of 0.2) as proposed by H. R. Griem⁵ agrees with the observed broadening for two elements of different electronic structure within experimental and theoretical accuracy, and the experimental lineshapes are not in disagreement with a Lorentz profile below the blackbody limit. (Note added in proof: Estimates⁷⁰ of the higher multipole contribution to the observed broadening amount to about 36% and are included in the semiempirical cross section quoted here, thus the conclusions presented here regarding the agreement between these results and the semiempirical estimates are unaltered. Calculation of the contribution due to Van der Waals broadening suggests a 10% correction while contributions due to resonance broadening and broadening by superelastic collisions are each about 3%.

The C II profile has since been rescanned two times by the author and does not show the large asymmetry reported here, the new profile fitting the factor-of-one curve very well, these newer results to be published soon.

The short wavelength shifts of the absorption dips of C II, suggested as Doppler in origin, are also of the same order of magnitude as reported by Greig, et al.,⁷¹ due to the plasma polarization shift.

Finally, purely quantum mechanical calculation of the broadening of ion lines due to elastic collisions by electrons have been done by O. Bely and H.R. Griem⁷⁰ for Mg II and by K. S. Barnes and G. Peach⁷² for Ca II.)

C. Future Experiments

Recent determinations^{64,65} of oscillator strengths suggest that theoretical and experimental line broadening due predominantly to elastic collisions may be compared for other transitions of N II and C II and for ions of other elements for which $\Delta E \geq 2 kT$. Measurements of the elastic broadening of neutral atoms in the neighborhood of threshold where the inelastic cross sections vanish, and at lower electron thermal energies, are possible for those transitions of neutral species for which accurate oscillator strengths are available and for which $\Delta E \geq 0.5 kT$.

SELECTED BIBLIOGRAPHY

1. H. R. Griem, Plasma Spectroscopy, McGraw-Hill, New York (1964).
2. H. R. Griem, Phys. Rev. Letters 17, 509 (1966).
3. J. Cooper, Phys. Rev. Letters 17, 991 (1966).
4. J. Cooper and G. K. Oertel, Phys. Rev. Lett. 18, 985 (1967).
5. H. R. Griem, Phys. Rev. 165, 258 (1967).
6. R. A. Day, Ph. D. Thesis, University of Maryland, 1965.
7. R. A. Day and H. R. Griem, Phys. Rev. 140, A1129 (1965).
8. C. H. Popenoe and J. B. Shumaker, Jr., J. Res. Natl. Bur. Std. 69A, 495 (1965).
9. N. W. Jalufka, G. K. Oertel, and G. S. Ofelt, Phys. Rev. Ltr. 16, 1073 (1966).
10. M. Yamamoto, Phys. Rev. 146, 137 (1966).
11. W. R. Powell, dissertation, Johns Hopkins University, 1966 (unpublished).
12. J. M. Bridges, dissertation, University of Maryland, 1966 (unpublished).
13. J. M. Bridges and W. L. Wiese, Phys. Rev. (in press).
14. D. E. Roberts, dissertation, Imperial College 1966 (unpublished).
15. J. R. Roberts and K. L. Eckerle, Phys. Rev. (in press).
16. M. J. Seaton in "Atomic and Molecular Processes," edited by D. R. Bates, Academic Press, Inc., New York (1962), Chap. 11.

17. H.R. Griem, paper presented at the "Eighth International Conference on Phenomena in Ionized Gases," Vienna 1967.
18. W.L. Wiese, M.W. Smith, and B.M. Glennon, National Standard Reference Data Series, National Bureau of Standards 4 (1966).
19. G.M. Lawrence and B.D. Savage, Phys. Rev., 141, 67 (1966).
20. R.C. Elton, Ph. D. Thesis, University of Maryland (1963).
21. R.C. Elton and H.R. Griem, Phys. Rev. 135, A1550 (1964).
22. R. Lincke, Ph. D. Thesis, University of Maryland (1964).
23. H. Petschek and S. Byron, Ann. Phys. 1, 270 (1957).
24. A. Unsold, Physik der Sternatmosphären, Chapter X and XI, Springer, Berlin (1955).
25. R.G. Breene, The Shift and Shape of Spectral Lines, MacMillan (Pergamon), New York (1961), also Line Width in Handbuch der Physik, Ed. S. Flugge, Vol. 27 p. 1, Springer, Berlin (1964).
26. G. Traving, Über die Theorie der Druckverbreiterung von Spektrallinien, G. Braun, Karlsruhe, (1960).
27. S. Ch'en and M. Takeo, Rev. Mod. Phys. 29, 20 (1957).
28. H. Margenau and M. Lewis, Rev. Mod. Phys. 31, 569 (1959).
29. M. Baranger, Phys. Rev. 111, 2, 481 (1959).
30. M. Baranger, Phys. Rev. 111, 2, 494 (1958).
31. M. Baranger, Phys. Rev. 112, 3, 855 (1958).

32. M. Baranger, Atomic and Molecular Processes, Ed. D. R. Bates, p. 493, Academic Press, New York (1962).
33. H. R. Griem, A. C. Kolb, and K. Y. Shen, Phys. Rev. 116, 4 (1959).
34. H. R. Griem, A. C. Kolb and K. Y. Shen, Astrophys. J. 135, 272 (1962).
35. H. R. Griem, M. Baranger, A. C. Kolb and G. Oertel, Phys. Rev., 125, 177 (1962).
36. H. R. Griem, Phys. Rev. 128, 515 (1962).
37. H. R. Griem, "Pressure Effects on Spectral Lines in a Plasma," International Conference on Optical Pumping and Atomic Line Shape, Warsaw, Poland (1968).
38. W. L. Wiese, Plasma Diagnostic Techniques, ed. R. H. Huddlestone and S.L. Leonard, Academic Press, N. Y. (1965).
39. M. J. Seaton, Proc Phys. Soc. 79, 1105 (1962).
40. H. A. Bethe, Ann. Physik 5, 325 (1930).
41. H. Van Regemorter, Astrophys. J. 136, 906 (1962).
42. J. W. Bond, Jr., K. M. Watson, J. A. Welch, Jr., Atomic Theory of Gas Dynamics, Addison-Wesley, Reading, Mass. (1965).
43. M. W. Drawin, P. Felenbok, Data for Plasmas in Local Thermodynamic Equilibrium, Gauthier-Villars, Paris (1965).
44. G. K. Oertel, Proc. 8th Conf. Int. Phen. Ion. Gases, Vienna, 1967. See also J. Cooper and G.K. Oertel, Phys. Rev. (1969) (in press).

45. H. R. Griem, Phys. Rev. 131, 1170 (1963).
46. R. W. P. McWhirter, Plasma Diagnostics Techniques, ed. R. H. Huddlestone and S. Leonard, Academic Press, New York (1965).
47. R. Mewe, Brit. J. Appl. Phys. 18, 107 (1967).
48. E. A. McLean, C. E. Faneuff, A. C. Kolb, and H. R. Griem, Phys. Fluids 3, 843 (1961).
49. W. Wiese, H. F. Berg, and H. R. Griem, Phys. Rev. 120, 1079 (1960).
50. R. C. Isler and D. E. Kerr, Phys. Fluids 8, 1176 (1965).
51. K. K. Eckerle and R. W. P. McWhirter, Phys. Fluids 9, 81 (1966).
52. E. A. McLean and S. A. Ramsden, Phys. Rev. 140, A1122 (1965).
53. T. N. Lie, A. W. Ali, E. A. McLean and A. C. Kolb, Phys. Fluids 10, 1545 (1967).
54. M. J. Rhee, T. N. Lie, E. A. McLean, "Local Thermal Equilibrium in Magnetically Driven Shock" presented at the American Physical Society Meeting, Miami, Fla. (Nov. 1968), Bull. Am. Phys. Soc., 13, 1518 (1968).
55. M. Pavlov and A. N. Prasad, Z. Physik 212, 266 (1968).
56. N. V. Utterback and T. Griffith, Jr., Rev. Sci. Instr. 37, (1966).
57. W. H. Lupton, "Fast Triggered Spark Switches for a Two Megajoule Capacitor Bank," Fifth International Conference on Ionization Phenomena in Gases, Munich, Germany, 1961; Amsterdam-North Holland Pub. Co., Vol II, pp. 2059-2068, (1961).

58. A.C. Kolb, Phys. Rev. 107, 345 (1957).
59. G.A.W. Rutgers and J.C. DeVos, Physica, XX, 715 (1954).
60. M. Pivovonsky and M.R. Nagel, "Tables of Blackbody Radiation Functions", The Macmillian Co., New York (1961).
61. J.T. Davies and J.M. Vaughan, Ap. J. 137, 1302 (1963).
62. P. Kepple and H.R. Griem, Phys. Rev. 173, 317 (1968).
63. R.L. Kelly, "Atomic Emission Lines Below 2000 Angstroms-Hydrogen through Argon," NRL Report 6648 (1968).
64. J.E. Hesser and B.L. Lutz, JOSA 58, 1513 (1968).
65. L. Heroux, Phys. Rev. 153, 156 (1967).
66. Numbers associated with the various data points correspond to the experimental references, and the lengths of the arrows indicate changes in the calculated widths when the total dipole strength is split into individual $i-i'$ contributions. The abscissa in all cases corresponds to the perturbing level closest to the upper level of the line, and the exponential curve gives an estimate of the inelastic contribution [Eq. (10)]. See also Ref. 5.
67. C.P. Lim, G.A. Moo-Young, G. Palumbo, J.R. Greig and H.R. Griem, Phys. Rev. 172, 148 (1968).
68. M.H. Miller and R.D. Bengtson, Bull. Am. Phys. Soc. 13, 1512 (1968).
69. H.R. Griem, Comments on Atomic and Molecular Physics, Gordon and Breach, N.Y. (to be published).

70. O. Bely & H.R. Griem, Phys. Rev. (January 1970).
71. R.L. Greig, L. Jones, T. Oda, H.R. Griem, Phys. Rev. Ltrs. (January 1970).
72. K.S. Barnes & G. Peach, Nature (in press).

DOCUMENT CONTROL DATA - R & D

(Security classification of title, body of abstract and indexing annotation must be entered when the overall report is classified)

1. ORIGINATING ACTIVITY (Corporate author) Naval Research Laboratory Washington, D.C. 20390		2a. REPORT SECURITY CLASSIFICATION Unclassified	
		2b. GROUP	
3. REPORT TITLE MEASUREMENT OF NITROGEN II AND CARBON II RESONANCE MULTIPLET LINE SHAPES FROM A PLASMA			
4. DESCRIPTIVE NOTES (Type of report and inclusive dates) Final report on one phase of a continuing problem.			
5. AUTHOR(S) (First name, middle initial, last name) Fortna, John D.E.			
6. REPORT DATE December 31, 1969		7a. TOTAL NO. OF PAGES 82	7b. NO. OF REFS 69
8a. CONTRACT OR GRANT NO. NRL Problem 77H02-24		9a. ORIGINATOR'S REPORT NUMBER(S) NRL Report 6950	
b. PROJECT NO. RR 002-09-41-5054		9b. OTHER REPORT NO(S) (Any other numbers that may be assigned this report)	
c.			
d.			
10. DISTRIBUTION STATEMENT This document has been approved for public release and sale; its distribution is unlimited.			
11. SUPPLEMENTARY NOTES		12. SPONSORING MILITARY ACTIVITY Department of the Navy (Office of Naval Research) Washington, D.C. 20360	
13. ABSTRACT The spectral line shapes of the Nitrogen II and Carbon II resonance multiplets, which occur in the vacuum ultraviolet region of the spectrum, have been measured. The Stark widths were deduced from the optically thin Lorentz wings. The source of radiation was a hot plasma produced by reflecting the shock wave generated by an electromagnetic T-type shock tube operating at a moderate pressure of helium gas to which the test elements (and hydrogen) were added. The electron temperature was determined from the ratio of the total intensities of the He I 4713 Å and the H β 4861 Å lines. The electron density was obtained from the halfwidth of the He I 3889 Å line. Measurement of the electron temperature and density of the test plasma was such as to provide a critical test of a recent semiempirical theory of Stark broadening of isolated ion lines under conditions in which the broadening electron collisions are predominantly <u>elastic</u> and without classical analogue. Agreement with the theory was found to within the expected precision of the theory.			

14. KEY WORDS	LINK A		LINK B		LINK C	
	ROLE	WT	ROLE	WT	ROLE	WT
Plasma generators Shock tubes Atomic spectroscopy Line spectra Line width Ultraviolet spectrum Visible spectrum Resonant frequency Ionized gases Nitrogen Carbon Elastic scattering Inelastic scattering						